ATMOSPHERIC ENVIRONMENT: X 30 (2026) 100433

Contents lists available at ScienceDirect

Atmospheric Environment: X

journal homepage: www.journals.elsevier.com/atmospheric-environment-x

Composition and radiative forcing of aerosols across the Indo-Gangetic Plain and Himalayas: A seasonal analysis

S. Ramachandran [a,b,*], Maheswar Rupakheti [b]

[a] Physical Research Laboratory, Ahmedabad, India
[b] Research Institute for Sustainability at GFZ Helmholtz Centre for Geosciences, Potsdam, Germany

ARTICLE INFO

Keywords:
Atmospheric aerosols
Chemical properties
Single scattering albedo
IGP and Himalayan foothills
Radiative effects
Climate implications

ABSTRACT

The chemical composition determines the influence atmospheric aerosols exert on environment, radiation budget, and climate. In this study, for the first time, using Aerosol Robotoc Network (AERONET) columnar aerosol observations at ten locations across the Indo-Gangetic Plain (IGP) and the Himalayan foothills, a comprehensive regional and seasonal analyses of aerosol chemical characteristics and radiative effects is performed. Single scattering albedo (SSA) increases during monsoon, with varying magnitude across the sites depending on the strength and the advancement of monsoon from west to east. SSA over Kathmandu in the Himalayan foothills during pre-monsoon is the lowest among all sites. Black carbon (BC) dominates aerosol absorption over the eastern IGP and the Himalayan foothills, whereas dust dominates the western IGP. Absorbing aerosol types are 'Mostly BC' and 'Mixed' which originate from urban/industrial and biomass burning emissions, and 'Mostly Dust' is absent over the eastern IGP and the Himalayan foothills revealing a spatial gradient in dust. Aerosol radiative forcing at the surface (ARF_{SFC}) is $\leq$ -50 Wm^{-2} throughout the year contributing to a significant surface cooling across the entire region. ARF efficiency at the surface and in the atmosphere are highest for Kathmandu. Aerosol-induced atmospheric solar heating rate (HR) is $\geq$ 0.4 K day^{-1} throughout the year at all sites. The HR is highest over Kathmandu (~1.5 K day^{-1}) during pre-monsoon. In present day conditions, a significantly regionally coherent higher HR over the Himalayas can enhance the total atmospheric warming in the large region. Quantitative knowledge obtained from the present analysis heretofore unavailable are crucial for global climate models and regional chemistry-transport models to more accurately assess the climate impact of aerosols over this ecologically sensitive and climatically vulnerable region.

1. Introduction

The size and chemical composition of atmospheric aerosols, emitted from natural sources and anthropogenic activities, which impact environment, human health, earth radiation budget, and climate, govern their chemical and physical characteristics. The chemical composition of aerosols depends on the types of aerosol species, which is based on the emission sources. The chemical composition of these aerosols comprising a mixture of light-scattering and absorbing particles, determine the extent of impact on environment and climate. These aerosols contribute to warming of the Earth's atmosphere and cooling at the surface. The net aerosol radiative forcing (ARF) is cooling, and has annulled a substantial portion of greenhouse gas warming (IPCC et al., 2021). Nevertheless, ARF is still a factor of three uncertain (IPCC et al., 2021). This uncertainty mainly arises from the inaccuracies involved in the determination of their chemical properties - aerosol absorption, and determination of the absorbing aerosol types (Myhre et al., 2013; Li et al., 2022). In global circulation/chemical transport models aerosol absorption is underestimated in many regions, in particular over Asia and at higher altitudes (Myhre et al., 2013; Shindell et al., 2013). The Indo-Gangetic Plains (IGP) which include parts of Pakistan, India, Nepal and Bangladesh, is a highly polluted, densely populated, intensely cultivated, and industrialized region. Diverse aerosol emissions from natural and anthropogenic sources (dust, black carbon, brown carbon, nitrate, sulfate and organics) give rise to a persistent blanket of haze with a peak in winter over this region and regions that are downwind (Lawrence and Lelieveld, 2010; Ramanathan et al., 2007).

The Himalayas and the surrounding regions have globally important yet frigile ecosystems and highly vulnerable population, and still, remain one of the less studied regions in terms of aerosols. The aerosol

* Corresponding author. Physical Research Laboratory, Ahmedabad, India.
E-mail address: ram@prl.res.in (S. Ramachandran).

https://doi.org/10.1016/j.aeaoa.2026.100433
Received 2 March 2026; Accepted 4 March 2026
Available online 11 March 2026

properties and trace gases over the Himalayan foothills and the Himalayas are largely affected by biomass burning emissions from northern India, southern Nepal and the Himalayan foothill region (Lüthi et al., 2015; Bhardwaj et al., 2018; Mahata et al., 2018; Singh et al., 2019). The emissions from forest fires, burning of crop waste, and bio-fuels used in cooking and heating also contribute to atmospheric aerosol composition over this region. In addition, atmospheric dynamics plays a dominant role in transporting and transforming the aerosols over this region (e.g., Lüthi et al., 2015; Singh et al., 2019). Air pollution over the Himalayas and the surrounding regions affects the health of large populace of people and ecosystems, crops, climate, cryosphere, precipitation and monsoon (e.g., Saikawa et al., 2019).

The simulation of aerosol characteristics in climate models remains a significant challenge, particularly in elevated locations such as the Himalayan-Tibetan Plateau region. The region's complex terrain, coupled with intricate vertical and horizontal transport processes (e.g., convection, large regional circulations, and local mountain-valley circulation), contributes to this complexity (Forster et al., 2021; Myhre et al., 2013). Evidence regarding the climate change over the Himalayas is still inconclusive, in particular aerosol-induced climate change, and estimates suffer from high uncertainty due to limited observational data (e.g., Krishnan et al., 2019; Forster et al., 2021). This is particularly true for the magnitudes and sign of regional aerosol distribution, their physical and chemical characteristics, and radiative forcing in both source, and downwind regions like the Himalayan mountain regions. (e.g., Krishnan et al., 2019; Forster et al., 2021).

Though satellites can provide global coverage on aerosols, the accuracy and resolution are lower (Schutgens et al., 2017). During the monsoon season, it is cloudy and overcast over the IGP, due to which satellite retrievals could be affected, as there exists no perfect cloud mask (Levy et al., 2013). Further, an uncertainty of ± 0.03 in MODIS AOD could be quite high to constrain aerosol forcing, therefore, MODIS AODs may be used as effectively to support studies that combine models, in situ observations and other satellite data sets for reducing the uncertainty (e.g., Levy et al., 2013). In addition, traditional satellite-based remote sensing observations can only retrieve fewer aerosol characteristics, for example AOD, as compared to ground-based measurements which remains a limitation. Aerosol extinction coefficient profiles from the Cloud-Aerosol Lidar and Infrared Pathfinder Satellite Observation (CALIPSO) are available at a 5-km horizontal resolution. However, CALIPSO takes 16 days to pass over the same location (i.e., about two over passes per month over a particular location), as a result its sampling frequency is lower (Gui et al., 2021).

Alternately, chemical analysis (e.g., Decesari et al., 2010) and/or source apportionment (Gustafsson et al., 2009; Chen et al., 2019) can be useful to ascertain the sources of aerosols over this region, however, these studies correspond to the surface whereas studies on columnar aerosols have not been performed so far over this region in a manner envisaged in this study, which would be very crucial for radiative forcing estimates and climate change assessments. The earlier studies over these regions (e.g., Kedia et al., 2014; Ramachandran and Kedia, 2012; Gautam et al., 2011; Gustafsson et al., 2009; Raatikainen et al., 2014; Cho et al., 2017; Rupakheti et al., 2019), were limited to (a) a particular season, (b) one or two locations in this region, (c) a small set of aerosol properties, and (d) surface or columnar measurements. Deriving aerosol characteristics and radiative effects are not only crucial but also challenging over the Himalayas due to its diverse sources, complex terrain, horizontal and vertical transport and mountain valley circulation (e.g., Lüthi et al., 2015). The regional scale investigations on the radiative forcing of aerosols over the IGP and the Himalayan foothills are indeed quite limited, and all the radiative forcing estimates obtained so far were based on the sensitivity analysis of a combination of aerosol chemical and optical properties in different radiative transfer models (Ramachandran and Kedia, 2012; Cho et al., 2017) which have significant uncertainties. Thus, determining the radiative effects of aerosols more accurately in order to obtain a realistic assessment of aerosol impacts over this region is crucial.

The present study comprehensively examines the seasonal variations in the chemical composition of columnar aerosols (single scattering albedo, refractive index), absorbing aerosol types, and radiative effects covering the entire IGP and the Himalayas, which are crucial for understanding climate change, air quality, and other environmental changes. The results are deduced from a detailed analysis of aerosol characteristics that is constrained (considering seasonal variations in upper and lower bounds of aerosol properties) by high-quality ground-based observations. The study's novelty lies in its observational data-intensive approach, and statistical robustness. It leverages new, high-quality ground-based column observations of multiple aerosol parameters from ten distinct locations (including recently established Aerosol Robotic Network (AERONET) sites in the Himalayan region), besides systematic confirmation of already established features, covering a large spatial domain within a climate-sensitive hotspot of global significance. This extensive dataset enables the identification of seasonal-scale variations with unprecedented accuracy. By presenting the observational evidences and constraints, this study provides critical insights that have significant implications for advancing aerosol science, refining climate models, and enhancing our understanding of regional and global climate change, particularly quantification of impacts of aerosols, a major current and future driver of regional climate change in South Asia.

2. Study locations and meteorology

Ten AERONET (Aerosol Robotic Network) (Holben et al., 2001) sites across the IGP and the Himalayan foothills: Karachi, Lahore and New Delhi in western IGP; Kanpur, Gandhi College, and Lumbini in central IGP; Dhaka and Bhola in eastern IGP; and Pokhara and Kathmandu in the Himalayan foothills (Fig. 1) were selected for the study. The selected study locations exhibit a widely varying environmental ambience (Fig. 1). The sites in Nepal are located at increasing altitudes, from ca. 100 m asl north of the IGP to the central Himalayan foothills with distinctly different physiographical settings and urbanization. Lumbini, is a rural area at the northern edge of the IGP, at the base of the Himalayan mountains to the north. The Kathmandu Valley and Pokhara Valley are the two metro regions situated in the Himalayan foothills. Lahore, New Delhi, Kanpur and Dhaka are metropolitan cities that are industrialized and marked with heavy air pollution (Fig. 1). Kanpur is located about 500 km east of the megacity New Delhi whereas Gandhi College is a rural location (~500 km to the east of Kanpur) and mostly downwind of Kanpur and New Delhi. Karachi is an urban, coastal city with two seaports. Bhola is the largest island in south-central Bangladesh and bounded by the Bay of Bengal in the south. The chosen study region experiences humid subtropical climate (hot, humid summer and cold, dry winter), and influenced by the South Asian monsoon system (Lawrence and Lelieveld, 2010; Kedia et al., 2014; Singh et al., 2019). The synoptic winter winds over the IGP and the Himalayas vary distinctly as a function of season – the winds are calm, and northerly/northeasterly during winter aiding the accumulation of local and regional emissions and giving rise to the annually recurrent atmospheric haze over the region, whereas during pre-monsoon, and monsoon (or rainy season) the winds originate from southwesterly direction, stronger than winter, and transport dust from arid regions (pre-monsoon), and sea salt from the surrounding oceans (Arabian Sea and Bay of Bengal), and mineral dust from the deserts. The winds undergo a directional transition as they change from southwest to northeast and are calmer than winter in post-monsoon. Further, the local/regional mountain-valley wind circulation and changes play a role in governing the air pollution over mountainous regions.

3. Data and analysis

The level 2, version 3 cloud screened and quality assured daily data of single scattering albedo (SSA), aerosol optical depth (AOD),

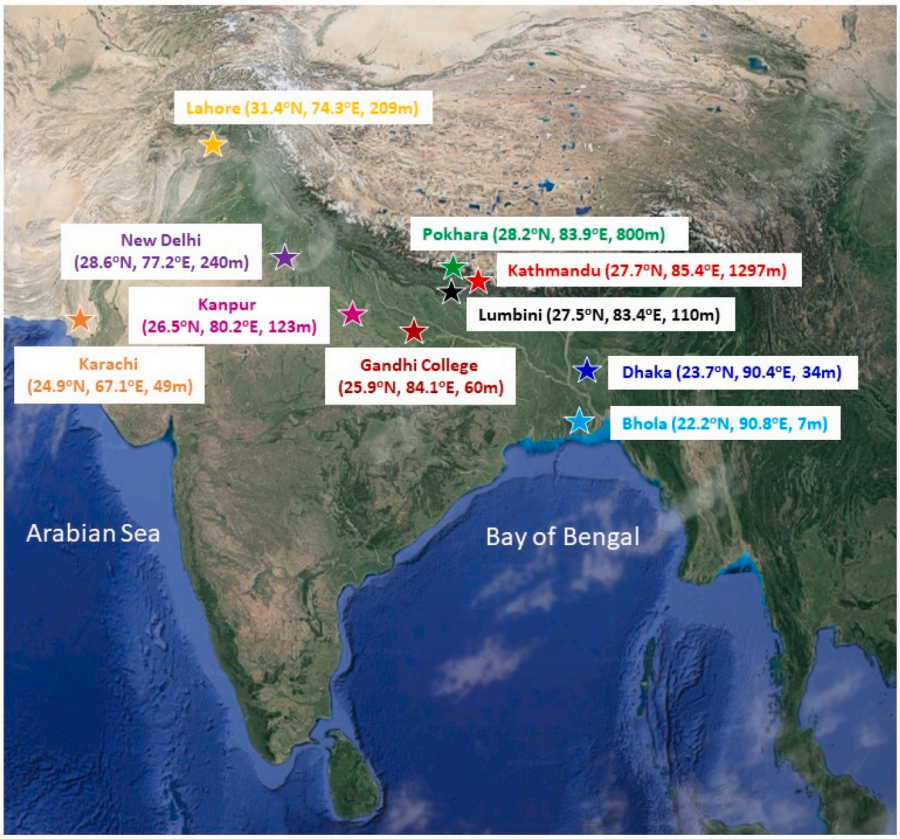

Fig. 1. Details of the study locations in the Indo-Gangetic Plains (IGP) and the Himalayan foothills (the background map was generated using Google maps (https://www.google.com/maps): Karachi, Lahore and New Delhi in western IGP; Kanpur, Gandhi College and Lumbini in central IGP; Dhaka and Bhola in eastern IGP; and Pokhara and Kathmandu in the Himalayan foothills. The latitude, longitude and elevation (in meters above sea level) of each location are also given in the figure.

absorption aerosol optical depth (AAOD), refractive index (real and imaginary parts), asymmetry parameter (*g*), fine mode fraction (FMF), Ångström exponent (AE), absorption Ångström exponent (AAE), extinction Ångström exponent (EAE), aerosol radiative forcing (ARF), and aerosol radiative forcing efficiency (ARFE) measured with ground-based Sun-sky photometer (Giles et al., 2019) for a period of a year, in Pokhara (2012 January-December), Bode, Kathmandu (2013 January-December), Karachi and Lahore (2012 January-December), New Delhi (2009 January-December), Lumbini (2013 January-August and 2017 September-December), Kanpur and Gandhi College (2012 January-December), and Dhaka (2014 January-December) and Bhola (2015 January-December) (Table 1), are analyzed. The main objective of the study was to cover all the seasons in a year (annual cycle) over all the study locations across the region, therefore, the above data sets corresponding to the years 2013-2015 were used; when data during 2013-2015 were unavailable, data from 2012 were used. This 3-year period (2012-2015) was chosen because concurrent data were available for almost all months at these locations only during this period over the region. For Delhi data for the entire year were available only for the year 2009, which are utilized. This approach of analyzing the data available in the preceding/ensuing year(s) with respect to the chosen year is quite suitable, robust, and is not expected to modify the scientific outcomes significantly as the data are from the same instrument, the seasonal variations in aerosols are more prominent than the year-on-year variations, and the influence of changes due to emissions and/or meteorology on aerosols is fairly small (Lawrence and Lelieveld, 2010; Kedia et al., 2014; Zhang et al., 2019). As the data over multiple sites for different years were unavailable simultaneously, statistical significance of interannual variations in aerosol properties could not be determined for each site. However, the inter-annual variability in aerosol properties during 2015-2019 over two sites in the IGP (Kanpur and Gandhi College) were found to be statistically insignificant as the p-value was >0.05 at 95% confidence level (calculated using two-tailed Student's t-test) (Ansari and Ramachandran, 2023). The number of days of daily-average data used as function of season (winter (DJF), pre-monsoon (MAM), monsoon (JJAS) and post-monsoon (ON)) corresponding to each location (mentioned in brackets) are - 83, 84, 70, and 57, (Pokhara), 81, 76, 59, and 41 (Kathmandu), 81, 80, 49, and 19 (Karachi), Lahore (58, 82, 107, and 56, (Lahore), 31, 46, 48, and 14 (New Delhi), 45, 78, 48, and 48 (Lumbini), 54, 72, 63, and 29 (Kanpur), 64, 82, 78, and 58 (Gandhi College), 76, 70, 52, and 54 (Dhaka) and 81,

Table 1
Threshold values of aerosol parameters used in the study to distinguish aerosol types (extinction Ångström exponent (EAE), refractive index – real part (RIR)), and absorbing aerosol types (fine mode fraction (FMF) and Ångström exponent (AE)).

Aerosol types	**EAE vs. RIR**	
	EAE	RIR
Biomass Burning (BB)	1.00-1.50	1.43-1.57
Urban/Industrial (UI)	0.70-1.74	1.35-1.43
Dust	0.01-0.41	1.44-1.59
Absorbing Aerosol types	**FMF vs. AE**	
	FMF	AE
Mostly Black Carbon (MBC)	0.70-1.00	1.00-1.50
Mostly Dust (MD)	0.10-0.40	0.00-0.40
Mixed (BC and Dust)	0.40-0.70	0.40-1.00

80, 37, and 48 (Bhola). Since, the study region is, in general, cloudy and overcast during monsoon, the number of days for which quality-control data are available is less in this season.

3.1. AERONET measurements

The field of view of the Sun/sky radiometer used in AERONET is 1.2°. The radiometer makes direct solar radiation measurements approximately every 15 min under clear-sky conditions, which typically results in about 20 measurements every day. The aerosol products derived from direct solar measurements at five spectral channels of 0.44, 0.50, 0.675, 0.87 and 1.02 μm, and sky radiance measurements made at four spectral channels of 0.44, 0.675, 0.87 and 1.02 μm are utilized in the study. The aerosol properties retrieved from AERONET measurements have the highest accuracy in the solar zenith angle range of 50° and 80° (Dubovik et al., 2000), and only those data points in a day that are within this solar zenith angle range are utilized in the study. The uncertainty in AODs from the direct solar radiation measurements is less than ±0.01 for wavelengths >0.44 μm (Holben et al., 2001). The error in AERONET derived FMF is ~10% (O'Neill et al., 2003). The error in SSA is ±0.03 when the AOD at 0.44 μm is > 0.2 (Dubovik et al., 2000). The uncertainty in AAOD is ±0.01 (Mallet et al., 2013). The uncertainty in the real and imaginary parts of refractive index are in the range of 0.025-0.05 and 30-50%, respectively (Dubovik et al., 2000). The uncertainty in asymmetry parameter (g) is ±0.02 (Dubovik et al., 2000). The spectral AOD, extinction AOD (EAOD) and AAOD follow a power law of the form, $x = K\lambda^{-\beta}$, where λ is the wavelength, x is AOD or EAOD or AAOD as the case may be, and β is AE or EAE or AAE, respectively. AE, EAE and AAE are estimated as slopes of linear regression between ln (AOD) and ln (λ), ln (EAOD) and ln (λ), and ln (AAOD) and ln (λ), respectively, in the wavelength range of 0.44−0.87 μm. AOD and EAOD, in principle, are the same as both represent the columnar extinction/attenuation of radiation by aerosols, however, they are retrieved using two different algorithms in AERONET (Dubovik et al., 2000). AOD is derived from the direct radiation measurements (direct Sun algorithm) while EAOD is retrieved from the direct and diffuse sky radiation measurements (solar almucantar scenario in inversion algorithm). Further, AE and FMF are derived from direct radiation measurements through direct Sun algorithm while AAOD, SSA, refractive index, asymmetry parameter and ARF are derived the direct and diffuse sky radiance measurements through the solar almucantar scenario in inversion algorithm.

3.2. Determination of aerosol type and absorbing aerosol type

Aerosol type: The matrix of aerosol properties retrieved by AERONET and their inter-relations (EAE vs. AAE, EAE vs. SSA, and EAE vs. refractive index – real part (RIR)) can be used to classify aerosols into different source types, such as originating from biomass burning, urban/industrial mix, and dust aerosols across the globe, emitting mostly BC, dust and a mixture of BC and dust, with respective threshold values primarily obtained from long-term observational data from reference sites characterized by different dominant aerosol types over the globe including USA, Europe, Africa and Asia (Russell et al., 2010, 2014; Giles et al., 2012; Rupakheti et al., 2019), and have been/are being used successfully and widely across the globe to classify the aerosol types. EAE represents the wavelength dependence of aerosol extinction, which is based on aerosol size distribution and varies depending on aerosol type and dominance (Russell et al., 2014), and AAE denotes the wavelength dependence of aerosol absorption. SSA (ratio of scattering AOD to total AOD), and the real part of RI depends on the chemical composition of aerosols, and is a measure of scattering due to aerosols. The relation between EAE and RIR is used to classify the aerosol types over the study region, because (a) EAE and RIR correspond to the total (composite) aerosols, as opposed to, the relation between EAE and AAE (absorption), and (b) the threshold values for EAE and RIR that are used to classify the aerosols as UI, BB and DU type (Table 1) do not overlap unlike the threshold values between EAE and AAE, and/or EAE and SSA (Table 1, Rupakheti et al., 2019). AE and EAE depend on aerosol size distribution; higher AE and EAE values (>1) indicate the dominance of fine mode aerosols (produced from combustion sources (e.g., coal fired power plants), industrial and vehicular emissions and domestic biomass burning (fuel wood and dung cake)), while lower AE and EAE (<1) occur due to the dominance of coarse mode aerosols (dust and sea salt) in aerosol size distribution. Thus, EAE values are >0.70 due to the dominance of fine mode aerosols from fossil fuel, industrial and biomass burning emissions whereas EAE for dust aerosol type is significantly lower because of dominant larger size coarse particles. The real part of refractive indices is lower for UI and BB aerosol types than dust type aerosols due to the dominant aerosol emissions from their respective sources – sulfate, black carbon arising from urban/industrial and biomass burning emissions while dust from deserts which has a higher real refractive index. The threshold ranges of refractive index for different aerosol types are consistent with observations as RIR was found to lie in the range of 1.40-1.47 for urban/industrial and mixed aerosols, between 1.47 and 1.52 for biomass burning aerosols and in the 1.36-1.56 range for desert dust (Dubovik et al., 2002). These distinct features in aerosol emissions from respective sources and their dominant sizes enable in determining the ranges of UI, BB and dust aerosol types (Table 1) and thereby identify the aerosol types.

Absorbing aerosol type: The uncertainty associated with identifying absorbing aerosol type, and their amount contributes majorly to the uncertainty in global ARF estimates (Li et al., 2022), and the uncertainty is expected to be even higher in heavily polluted regions (Ramanathan et al., 2007; Myhre et al., 2013; Li et al., 2022). This uncertainty arises mainly due to the anthropogenic absorption AOD, and mainly due to the uncertainty in BC. Among the absorbing aerosols, BC absorption is at least 4-times (SSA~0.20) higher than BrC and dust (SSA~0.85). Though BC contributes less to aerosol mass (5-10%), compared to BrC (16%) and dust particles (35%) over South Asia (Jimenez et al., 2009; IPCC et al., 2021), however, as its absorption is significantly stronger, it is arduous to derive the relative contribution of absorbing aerosols to absorption, and ARF. Furthermore, BrC absorption is wavelength dependent, effective over the 0.3-0.6 μm wavelength range, with its absorption falling very sharply beyond 0.4 μm. BrC contributes <5% to total light absorption beyond 0.55 μm (Kirillova et al., 2016). Since, the radiative effect of BC is at least 4-times stronger than that of the other absorbing aerosol species (dust and BrC), and as BrC contribution to light absorption is significantly less, it is vital to differentiate and quantify the major absorbing aerosol types (BC and dust).

The absorbing aerosol types are classified into three as – *mostly dust* (MD), where iron oxide in dust is dominant absorber, *mostly BC* (MBC), consisting of mixture of biomass burning and urban/industrial emissions in which BC is the dominant absorber, and *mixed*, corresponding to the optical mixture of BC in fine mode and dust in coarse mode dust as dominant absorbers (Giles et al., 2012). The relations between AE and FMF, SSA and FMF, and AAE and FMF are being effectively and widely used to derive the absorbing aerosol types in the atmosphere using large number of long-term observational datasets from the reference sites characterized by different dominant absorbing aerosol type spread over the globe (USA, Europe, Africa and Asia) (Giles et al., 2019; Rupakheti et al., 2019), and are being utilized effectively to document the absorbing aerosol types. AE and FMF are closely linked – AE (>1) and FMF (>0.7-1.0) will be higher when fine mode aerosols dominate the aerosol distribution, while both AE and FMF will be lower (<0.5) when coarse mode aerosols dominate. For a mixed (fine plus coarse) aerosol distribution AE and FMF will lie between the above two ranges. Urban/industrial and biomass burning emissions dominantly produce aerosols in fine mode and mostly black carbon (MBC) giving rise to higher AE and FMF whereas when dust aerosols dominate AE and FMF are lower. In a mixture, BC in fine mode and dust in coarse mode will be present due to which the AE and FMF values will lie between the MBC

and dust absorbing aerosol types. The relation between AE and FMF is used in the study to classify the absorbing aerosol types, as in this classification also, both AE and FMF pertain to total (composite) aerosols, and the threshold limits for different absorbing aerosol types do not overlap (Table 1), unlike in case of the relations between AAE vs. FMF - AAE: 1.00-2.00 and FMF: 0.50-1.00 for MBC, AAE: 2.00-3.00 and FMF: 0.10-0.30 for MD, and AAE: 1.00-2.00 and FMF: 0.17-0.40 for Mixed; and in case of SSA vs. FMF – SSA: 0.84-0.97 and FMF: 0.50-1.00 for MBC, SSA: 0.90-0.95 and FMF: 0.10-0.40 for MD, and SSA: 0.84-0.90 and FMF: 0.20-0.50 for Mixed (Giles et al., 2012; Rupakheti et al., 2019). The role and influence of BrC in light absorption in this study is not included owing to the above, and due to that fact in the present study the classification into different aerosol types and absorbing aerosol types is based on composite (or total) aerosols and not on absorption AOD (Ramachandran et al., 2020) which is needed to estimate the influence of BrC on light-absorption.

3.3. Estimation of aerosol radiative forcing efficiency and heating rate

The ARF depends on the aerosol optical properties (which are governed by physical and chemical properties) (AOD, SSA, *g*), geophysical properties (surface albedo), and solar zenith angle. The surface albedo is not critical in accurately estimating ARF when it is < 0.30 but it is critical when it is above 0.30 (García et al., 2012). The ARF at the surface (ARF_{SFC}) in case of AERONET is overestimated as the fluxes with and without aerosols in the upward direction are not considered. This overestimate can be corrected by multiplying the ARF_{SFC} with 1-SA, where SA is the spectral average of surface albedo in the 0.34-1.02 μm wavelength region (García et al., 2012). The spectral average surface albedo in this region is < 0.30 during the year (Table 2), nevertheless, the surface albedo correction is implemented in the study to obtain a more accurate ARF. The surface albedo is higher over western and central IGP than the eastern IGP and the Himalayan foothills during pre-monsoon and monsoon than post-monsoon and winter.

The difference between ARF at the surface (ARF_{SFC}) and the ARF at the top of the atmosphere (ARF_{TOA}) is the ARF of the atmosphere (ARF_{ATM}). Subsequently, the aerosol-induced atmospheric solar heating rate (HR) is estimated as,

$$\frac{\partial T}{\partial t} = \frac{g}{c_p}\left[\frac{ARF_{ATM}}{\Delta P}\right] \quad (1)$$

where $\partial T/\partial t$ corresponds to the heating rate (in Kelvin (K) day^{-1}), g represents the acceleration due to gravity, the specific heat capacity of air at constant pressure is given as c_p, and ΔP is the pressure difference between the elevation of each location (Table 2) and the upper bound altitude up to which aerosols are present. Generally, a uniform upper bound of 3 or 5 km of the atmosphere above the earth's surface is used, based on the assumption that within this altitude range almost all the aerosols are present in the atmosphere, to determine the aerosol-induced aerosol heating rate (Ramanathan et al., 2007; Ramachandran and Kedia, 2012). This assumption is valid when aerosols are vertically uniformly distributed throughout this layer, which usually, is not the case over the IGP and the Himalayas. Therefore, a climatology of aerosol extinction profiles from CALIPSO retrieved during 2012-2015 (corresponding to the study period) is used to determine the seasonal mean upper height/bound relative to the surface pressure for each study location for estimating the aerosol-induced heating rate (Section 4.4, Table 3).

Table 2
Seasonal mean surface albedo over the study locations (latitude, longitude, elevation in meters (m) above mean sea level).

Location	Winter	Pre-monsoon	Monsoon	Post-monsoon
Himalayan foothills:				
1 Pokhara, Nepal (28.2°N, 83.9°E, 800m)	0.14 ± 0.01	0.16 ± 0.01	0.18 ± 0.01	0.16 ± 0.01
2 Kathmandu, Nepal (27.7°N, 85.4°E, 1297m)	0.15 ± 0.01	0.18 ± 0.01	0.20 ± 0.01	0.18 ± 0.01
Western IGP:				
3 Karachi, Pakistan (24.9°N, 67.1°E, 49m)	0.24 ± 0.01	0.25 ± 0.01	0.25 ± 0.01	0.24 ± 0.01
4 Lahore, Pakistan (31.4°N, 74.3°E, 209m)	0.19 ± 0.02	0.20 ± 0.01	0.21 ± 0.02	0.19 ± 0.02
5 New Delhi, India (28.6°N, 77.2°E, 240m)	0.16 ± 0.01	0.18 ± 0.02	0.20 ± 0.02	0.17 ± 0.01
Central IGP:				
6 Lumbini, Nepal (27.5°N, 83.3°E, 110m)	0.21 ± 0.02	0.22 ± 0.02	0.25 ± 0.02	0.22 ± 0.02
7 Kanpur, India (26.5°N, 80.2°E, 123m)	0.22 ± 0.02	0.23 ± 0.02	0.24 ± 0.02	0.22 ± 0.02
8 Gandhi College, India (25.9°N, 84.1°E, 60m)	0.22 ± 0.02	0.22 ± 0.02	0.23 ± 0.02	0.22 ± 0.03
Eastern IGP:				
9 Dhaka, Bangladesh (23.7°N, 90.4°E, 34m)	0.13 ± 0.01	0.15 ± 0.01	0.14 ± 0.01	0.13 ± 0.01
10 Bhola, Bangladesh (22.2°N, 90.8°E, 7m)	0.18 ± 0.01	0.21 ± 0.01	0.21 ± 0.01	0.22 ± 0.01

4. Results and discussion

4.1. AOD, SSA, AAOD, and refractive index

Aerosol optical depths in the 0.44-1.02 μm wavelength range are ≥0.3 over all the locations the entire year (Fig. 2), confirming that the entire region is heavily polluted. AODs exhibit significant spectral and seasonal variations (Fig. 2). AODs over Pokhara and Kathmandu, in the

Table 3
Seasonal mean altitudinal upper bound (in km) at each location, which corresponds to the altitude up to which aerosol extinction contributes ~99.5% to column aerosol extinction.

Location	Winter	Pre-monsoon	Monsoon	Post-monsoon
Himalayan foothills:				
1 Pokhara, Nepal (28.2°N, 83.9°E, 800m)	4.11	5.31	5.01	3.99
2 Kathmandu, Nepal (27.7°N, 85.4°E, 1297m)	4.65	5.97	6.99	4.29
Western IGP:				
3 Karachi, Pakistan (24.9°N, 67.1°E, 49m)	4.23	5.19	5.55	4.29
4 Lahore, Pakistan (31.4°N, 74.3°E, 209m)	5.07	6.75	5.79	5.01
5 New Delhi, India (28.6°N, 77.2°E, 240m)	4.53	5.49	5.31	3.87
Central IGP:				
6 Lumbini, Nepal (27.5°N, 83.3°E, 110m)	4.11	5.31	5.01	3.99
7 Kanpur, India (26.5°N, 80.2°E, 123m)	3.69	5.43	4.95	3.75
8 Gandhi College, India (25.9°N, 84.1°E, 60m)	3.69	5.43	4.95	3.75
Eastern IGP:				
9 Dhaka, Bangladesh (23.7°N, 90.4°E, 34m)	3.93	5.01	6.93	4.35
10 Bhola, Bangladesh (22.2°N, 90.8°E, 7m)	4.41	5.07	6.45	3.99

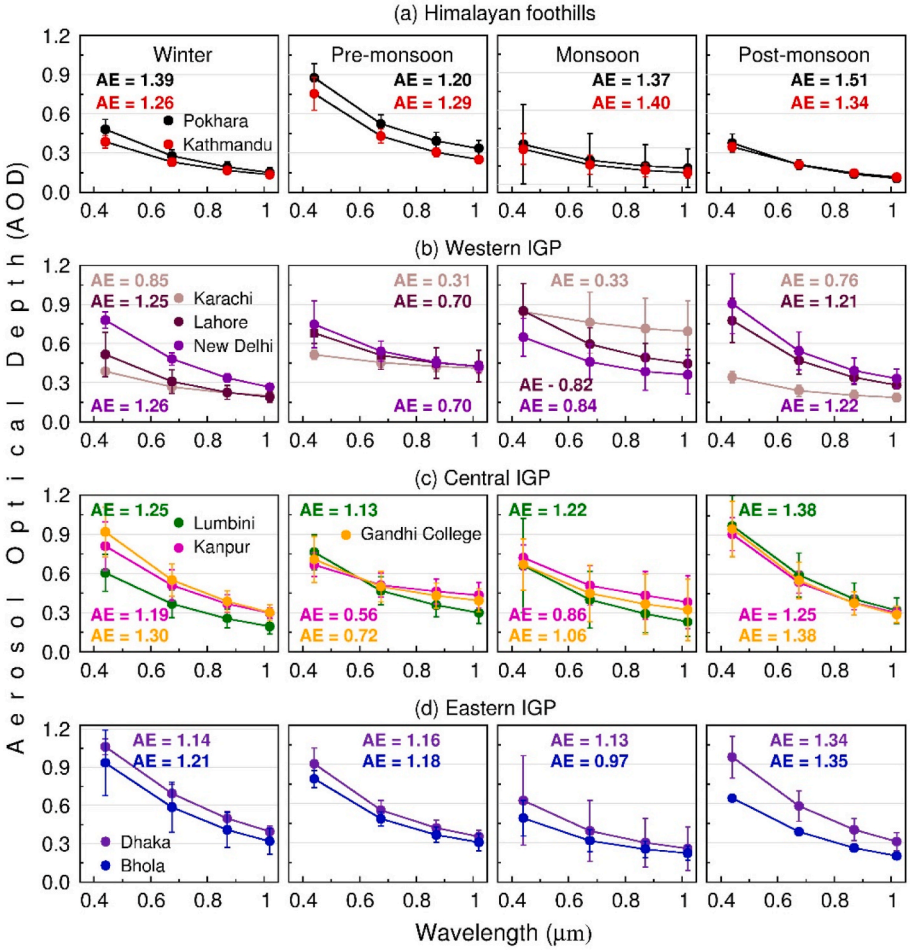

Fig. 2. Seasonal mean aerosol optical depth in the 0.44-1.02 μm wavelength region over the study locations in – (a) Himalayan foothills (Pokhara and Kathmandu in Nepal), (b) western IGP (Karachi and Lahore in Pakistan, and New Delhi in India), (c) central IGP (Lumbini in Nepal, and Kanpur and Gandhi College in India), and (d) eastern IGP (Dhaka and Bhola in Bangladesh), respectively. Vertical bars denote the ±1σ (standard deviation) from the seasonal mean. Seasonal mean Ångström exponent (AE) values for the study locations are given in the respective figure.

Himalayan foothills, are highest in pre-monsoon, lowest in monsoon and lie in between during post-monsoon, whereas Lumbini in Nepal has the highest AOD in post-monsoon followed by pre-monsoon, monsoon and winter (Fig. 2). Karachi AE values are the lowest in the entire IGP confirming the dominance of coarse mode particles throughout the year (Fig. 2). AE values are in general higher during winter and post-monsoon revealing the dominance of fine mode aerosols in these seasons. AE values are >1 over Pokhara, Kathmandu and Lumbini throughout the year revealing a consistent dominance of fine mode aerosols up to the northern edge of IGP and the Himalayas.

The spectral variation of SSA (0.44-1.02 μm wavelength region) depends on the dominant aerosol type in the atmosphere; SSA decreases with increasing wavelength for continental aerosols and biomass burning-influenced aerosols whereas SSA will increase with wavelength when dust dominates (Eck et al., 2005; Russell et al., 2010; Kedia et al., 2014). Further, SSA of dust is higher than continental and biomass burning aerosols. An almost linear SSA spectra (SSA independent of wavelength) suggest the presence of same type(s) or mixtures of aerosol species, and that the species also maintain their respective proportions (scattering vs. absorbing species) in the total in this wavelength region. The SSA and its spectral shape (independent, or decreasing or increasing as a function of wavelength) exhibit significant spatio-temporal variations across the region, however, over each sub-regional bound (i.e., western IGP, central IGP etc.) they are more or less the same (Fig. 3). All the three spectral shapes are present over the IGP and the Himalayan foothill regions during the year.

Over the sites in the western IGP (i.e., Karachi, Lahore, and New Delhi) which are influenced by dust, SSA typically increases with wavelength during the year (except over New Delhi during post-monsoon and winter); the increase in SSA being steeper during pre-monsoon and monsoon than post-monsoon and winter because of increased abundance of dust. The SSA (in all four wavelengths) over New Delhi is lowest, and the decrease as a function of wavelength is the steepest during post-monsoon among all the study locations. Over Kanpur, Gandhi College and Lumbini in central IGP (Fig. 1), SSA decreases slightly with wavelength during winter, increases during pre-monsoon and monsoon (except Lumbini), and decreases slightly again during post-monsoon (Fig. 3). Over the sites in eastern IGP, i.e., Dhaka and Bhola, SSA values are quite close to each other, and are either almost invariant as a function of wavelength or decrease slightly as a function of wavelength (post-monsoon, Fig. 3d). In an atmosphere dominated by fine mode aerosols AODs fall steeply with respect to wavelength ($AOD_{0.44\ \mu m}$ is $\geq$ 3 times $AOD_{1.02\ \mu m}$) as seen over the Himalayan foothills (Fig. 2), however, when dust is present the AOD spectra is less steep as in case of Karachi ($AOD_{0.44\ \mu m}$ is $\leq$ 2 times $AOD_{1.02\ \mu m}$; during monsoon AODs at 0.44 and 1.02 μm are almost comparable indicating the dominance of coarse mode particles). Kathmandu, whose elevation despite being higher than Pokhara exhibits lower SSA. Vertical profile measurements over and around the Pokhara valley revealed that the BC concentration at elevated locations in the Himalayas was higher than at the surface (Singh et al., 2019), leading to lower SSA values (Fig. 3). Absorption AOD (AAOD) over Pokhara is lower than Kathmandu

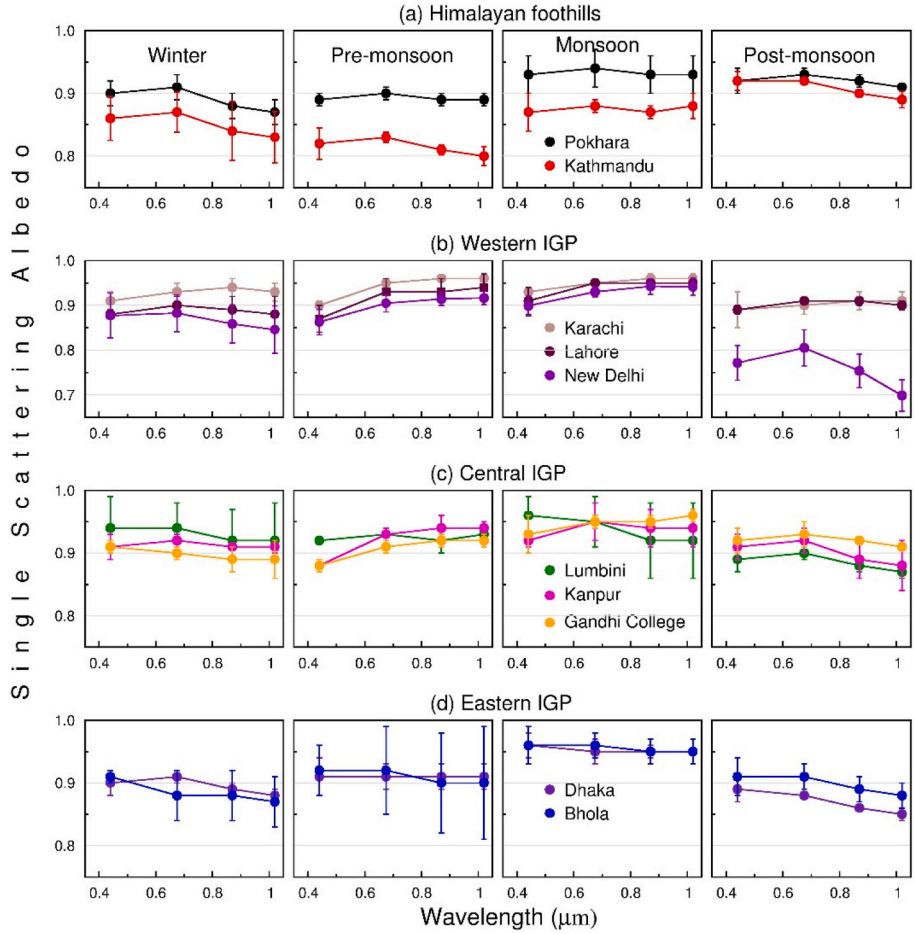

Fig. 3. Seasonal mean single scattering albedo (SSA) in the 0.44-1.02 μm wavelength region over the study locations in – (a) Himalayan foothills (Pokhara and Kathmandu in Nepal), (b) western IGP (Karachi and Lahore in Pakistan, and New Delhi in India), (c) central IGP (Lumbini in Nepal, and Kanpur and Gandhi College in India), and (d) eastern IGP (Dhaka and Bhola in Bangladesh), respectively. Vertical bars denote the ±1σ (standard deviation) from the seasonal mean.

confirming that the absorption (due to BC, Brown Carbon and dust aerosols) is relatively lower over Pokhara (Fig. 4) resulting in higher SSA over Pokhara.

SSA values increase at all locations during monsoon than the other seasons, however, the magnitudes of increase in SSA values differ (Fig. 3). The SSA values can increase or decrease depending on precipitation; SSA increases from west to east; the increase in SSA is relatively higher in Dhaka and Bhola than other locations. The SSA is higher over Bhola and Dhaka as compared to the other sites in IGP, with a more pronounced increase during monsoon compared to other locations. Rainfall across the IGP exhibits considerable spatial variability, decreasing by a factor of 2 to 3 from the east to west. For instance, in 2012, rainfall in Lahore was 360 mm, 822 mm in Kanpur, and 1257 mm in Dhaka. Consequently, the greater summer monsoon rain over eastern IGP, wet removal (AODs are lower than pre-monsoon (Fig. 2)) and sea salt particles result in higher SSA than the other IGP locations to the west of IGP like Kanpur and Lahore. Further, a higher RH during monsoon months (RH is 80% or higher across the study region (Ramachandran and Kedia, 2012)) aids the hygroscopic growth of aerosols resulting in higher SSA. The SSA increases with wavelength in pre-monsoon and monsoon owing to the increase in dust particles (coarse mode), as dust particles scatter radiation more efficiently beginning from 0.5 μm. The lowest SSA over New Delhi during post-monsoon is attributed to the transport of aerosols emitted by intensive agro-residue burning (which dominantly have light-absorbing BC aerosols followed by brown carbon (BrC) aerosols (Gustafsson et al., 2009)) in this season (Jethva et al., 2018). AODs at wavelengths shorter than 0.675 μm are significantly higher than longer wavelength AODs over the IGP and the Himalayan foothills during winter and post-monsoon consistent with higher amount of fine mode absorbing aerosols (lower SSA) except in Karachi (dust dominance) (Fig. 3) and over Kathmandu during pre-monsoon when SSA is the lowest among all the locations. $AOD_{0.44}$ averaged across the IGP and the Himalayan foothills is ≥ 3 times higher than $AOD_{1.02}$ during winter and post-monsoon confirming the dominance of fine mode aerosols in the atmosphere over this region whereas $AOD_{0.44}$ is only a factor of 2 higher than $AOD_{1.02}$ in pre-monsoon and monsoon when coarse mode (dust and sea salt) aerosols dominate (Fig. 2).

Results from the present study are compared with a couple of studies on aerosol optical properties conducted earlier in the Himalayan foothills and the mountain region. SSAs analyzed during a pre-monsoon campaign in the Himalayan foothills during 2009 - at Hetauda (27.4°N, 85.0°E, 465 m asl) during 18 Apr-30 May, and Dhulikhel 27.6°N, 85.5°E, 1500 m asl), both in HImalayan foothills, during 11 Apr-16 Jun in Nepal, were reported earlier in Gautam et al. (2011). The SSA at 0.44 μm was found to be < 0.90 over Hetauda and Dhulikhel (0.86 and 0.88 respectively) (Gautam et al., 2011). The shape of SSA spectra observed over Hetauda was quite similar to that observed over Gandhi College, a rural location in the central IGP influenced by dust, where the SSA increased from 0.88 (at 0.44 μm) to 0.90 (at 1.02 μm), while over Hetauda SSA increased from 0.86 to 0.89 at the respective wavelengths. The increase in SSA at longer wavelengths is most likely due to dust that was transported in addition to emission from soils disturbed by human activities (Gautam et al., 2011) (also seen in Fig. 3). Due to the presence of a mixture of local pollution transported upslope from Kathmandu

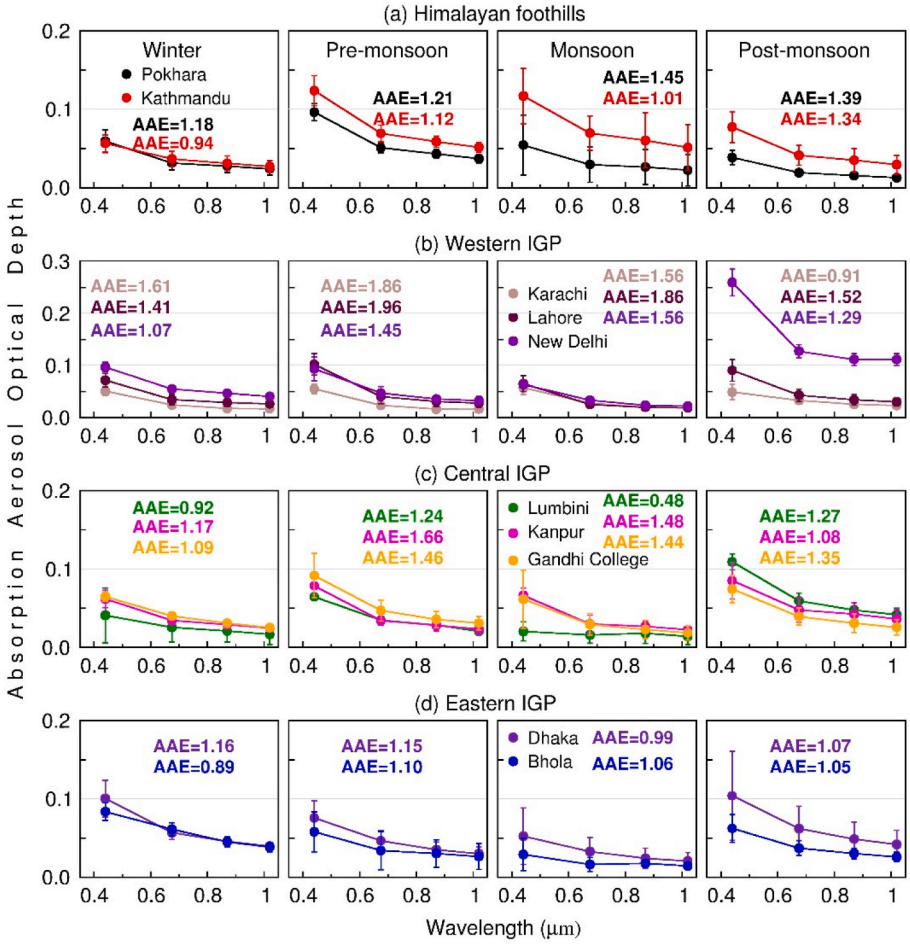

Fig. 4. Seasonal mean absorption aerosol optical depth (AAOD) in the 0.44-1.02 μm wavelength region over the study locations in – (a) Himalayan foothills, (b) western IGP, (c) central IGP, and (d) eastern IGP. Vertical bars denote the ±1σ (standard deviation) from the seasonal mean. Seasonal mean absorption Ångström exponent (AAE) values for the study locations are given in the respective figure.

Valley (fine) and transported dust (coarse), the SSA spectra is relatively flat over Dhulikhel (Gautam et al., 2011 and references therein). Whereas the SSA spectra are either flat or decrease with wavelength over the three study locations in Nepal with elevations varying from 110 m to ~1300 m asl in all the seasons (Fig. 3) similar to Dhulikhel (1500 m asl), suggesting that the contribution of dust particles to aerosol composition in the Himalayan mountain regions is less. SSA was in the 0.85-0.87 range over the northern peninsular Southeast Asia, a major biomass-burning hotspot region (Pani et al., 2018). The SSA values obtained over Kathmandu in this study compare well with SSA obtained over Southeast Asia influenced strongly by biomass burning emissions.

AERONET retrieved SSA over Dushanbe in Central Asia (38.6°N, 68.9°E, 821 m asl), located in the vicinity of Taklamakan, Karakum, and Aralkum deserts, was ≥0.90 throughout the year (Rupakheti et al., 2020). The SSA in winter was lower (0.90) suggesting the presence of more light-absorbing aerosols during winter whereas in the other seasons SSA was higher and increased with increasing wavelength due to the abundance of coarse mode dust particles (Rupakheti et al., 2020). This feature in SSA was consistent with the fine mode fraction (FMF) values, which were 0.77 (winter), 0.50 (spring), 0.39 (summer), and 0.50 (autumn) (Rupakheti et al., 2020). The increasing anthropogenic emissions in winter gave rise to higher FMF and lowest SSA (Rupakheti et al., 2020). The seasonal (winter low) and spectral (increasing SSA with increasing wavelength) SSA features over Dushanbe, attributed to dust aerosols in the atmosphere, are similar to the IGP and the Himalayan foothills. In Minsk, Belarus (53.9°N, 26.6°E, 235 m asl), SSA decreased with increasing wavelength throughout the year in all the seasons as the aerosol loading over Minsk was dominated by anthropogenic emissions, mainly BC (Filonchyk et al., 2021). On a seasonal scale SSA in summer > spring > autumn > winter over Minsk. The SSA in winter over Minsk was also the lowest (0.89) similar to the IGP and Dushanbe.

The AAOD (defined as (1-SSA) multiplied by AOD) exhibits a behavior opposite to that of SSA. A higher AAOD results in lower SSA, and *vice versa* (Fig. 4), because an increase in absolute content of light-absorbing aerosols in air directly increases AAOD and thereby SSA decreases. Among all sites, AAOD over New Delhi during post-monsoon is the highest followed by Kathmandu during pre-monsoon (resulting in the lowest SSA (Fig. 3)). The variations in AAE (spectral exponent of AAOD) can help identify potential aerosol sources and types. The value of AAE, an indicator of aerosol composition, varies between <1 and >2 (Russell et al., 2010). AAE of 1 or less indicates that the aerosol absorption is dominated by BC, and AAE of 1.5 indicates biomass burning aerosols, and when mineral dust particles dominate AAE value becomes 2 or even greater (Russell et al., 2010). The seasonal average AAE values are between 1 and 2 (except a few cases with AAE<1) (Fig. 4). In the Himalayan foothills, the AAE values between 1 and 1.5 over Pokhara and Kathmandu indicate that BC dominates aerosol absorption in the Himalayan foothills. In the western IGP, AAE values close to 2 over Karachi and Lahore during pre-monsoon categorically confirms the dominance of dust particles; AAE values reduce slightly during monsoon (1.6-1.9) (Fig. 4). SSA over Karachi is higher during winter than post-monsoon (Fig. 3); AAE is ~1 for Karachi in post-monsoon while it is 1.6 in winter, the lower AAE during post-monsoon suggesting an

increase in the abundance of BC. Similar is the case over New Delhi, Kanpur and Gandhi College during pre-monsoon and monsoon when dust abundance increases leading to higher AAE. The AAE over Lumbini during monsoon (0.48) is the lowest among all sites, an indication of BC-rich local emissions. The AAE values over the eastern IGP (Dhaka and Bhola) are around 1 throughout the year suggesting that aerosol absorption is mostly dominated by BC (Fig. 4).

The strong convection in the pre-monsoon season aids air masses with pollution to get lifted to higher heights and advect northwards towards Himalayas (Lüthi et al., 2015; Singh et al., 2019). The horizontal movement (advection) of air masses during pre-monsoon is also aided by the strong updraft and a higher atmospheric boundary layer. The advected polluted air masses often get mixed with synoptic scale westerlies (Raatikainen et al., 2014; Putero et al., 2018; Singh et al., 2019), and give rise to the lowest SSA during pre-monsoon over Kathmandu. The emissions from forest fires and the subsequent transport get suppressed due to monsoon rains, and brick production in IGP and the valleys in the Himalayan foothills are less active in this season. Due to wet removal, suppression of transport of regional emissions, and less active local scale major seasonal sources such as forest fires and brick production result in higher SSA over Lumbini and Pokhara, however, SSA is still lower over Kathmandu clearly confirming the presence and dominance of BC aerosols (which have the lowest SSA among all aerosol types) even at higher altitudes of the Himalayan foothills, which is consistent with the changes in AAOD and AAE (Fig. 4).

The insights on aerosol absorption can be expanded by analyzing the aerosol refractive index (RI) - real and imaginary parts. The real part of RI denotes the scattering contribution, whereas the imaginary part represents the absorption contribution, and thus, the real and imaginary parts depend on the chemical composition of aerosols. The real part of RI is found to lie in the range of 1.40-1.47 for urban/industrial and mixed aerosols, between 1.47 and 1.52 for biomass burning aerosols and in the 1.36-1.56 range for desert dust, whereas their imaginary equivalents were between 0.003 and 0.014, 0.00093 and 0.021, and 0.0007 and 0.029, respectively for the above aerosol types (Dubovik et al., 2002). The real and imaginary parts of RI differ on a seasonal scale (Figs. 5 and 6) consistent with SSA variation (Fig. 3) across the IGP and the Himalayan foothills. The real part of RI over Pokhara and Kathmandu is in the 1.40-1.55 range (Fig. 5) while the imaginary RI is in the 0.005-0.02 range (Fig. 6), indicating the dominance of aerosols from biomass burning and urban industrial activities. SSA is lowest over Kathmandu during pre-monsoon (Fig. 3) which increased during monsoon. The real part of RI over Kathmandu is $>$ 1.5 during pre-monsoon and monsoon with pre-monsoon RI being slightly higher (Fig. 5a), while the imaginary part of RI during pre-monsoon ($\geq$0.2) is significantly higher than monsoon ($\sim$0.01) (Fig. 6a). SSA is lower in pre-monsoon than monsoon over Kathmandu because of the more prominent increase in the absorbing aerosols from local (brick production, diesel generator sets) and regional (forest fires, agro-residue fires) as revealed by lower imaginary part of RI. In western IGP the real and imaginary refractive index over Karachi and Lahore are comparable (Figs. 5b and 6b). The real part is $>$ 1.45 over both the locations whereas the imaginary part is $<$ 0.02; the imaginary parts of RI are lowest during pre-monsoon and monsoon due to higher amount of dust which effectively scatter more light at longer (infrared) wavelengths and this is evident in higher SSA (Fig. 3). The features in RI over New Delhi are comparable to that of

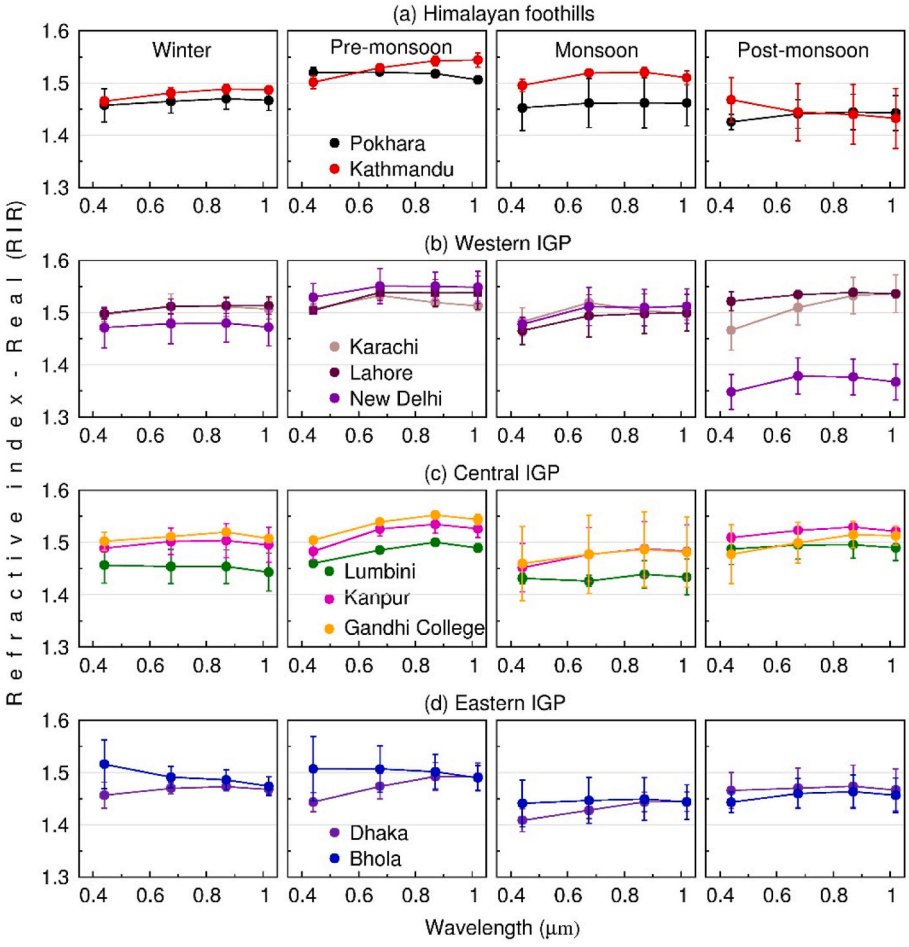

Fig. 5. Real part of refractive index (RIR) of aerosols in the 0.44-1.02 μm wavelength range over the study locations in the (a) Himalayan foothills, (b) Western IGP, (c) Central IGP and the (d) Eastern IGP. The ±1σ (standard deviation) from the seasonal mean is denoted by vertical bars.

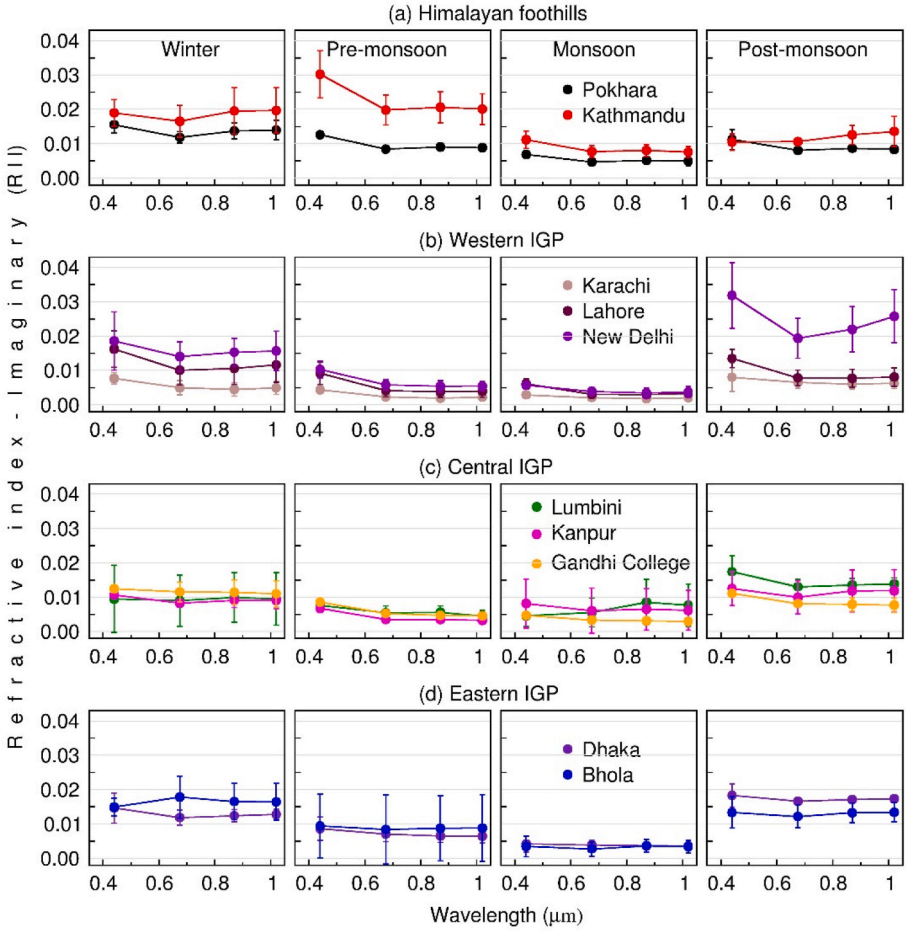

Fig. 6. Imaginary part of refractive index (RII) of aerosols in the 0.44-1.02 μm wavelength range over the study locations in the (a) Himalayan foothills, (b) Western IGP, (c) Central IGP and the (d) Eastern IGP. The ±1σ (standard deviation) from the seasonal mean is denoted by vertical bars.

Lahore and Karachi, with an exception over New Delhi during post-monsoon which has lower real part and higher imaginary part than other two sites in western IGP. The significant decrease in the real and the significant increase in the imaginary parts of RI during post-monsoon over New Delhi emphasizes that the dominant aerosol type changed from dust (monsoon) to BC (post-monsoon) leading to a significant decrease in SSA (the lowest during post-monsoon) (Fig. 3). Over the central IGP, Kanpur, Gandhi College and Lumbini all have similar features in both real and imaginary parts. The real part of RI decreases significantly to <1.45 over Lumbini in monsoon (values are in the 1.45-1.60 during the other seasons) (Fig. 5c), and the imaginary part increases to ≥0.2 in post-monsoon (values are <0.02 during the other seasons) (Fig. 6c). The real part of RI over Dhaka and Bhola in Bangladesh is lower during monsoon and post-monsoon than the other two seasons, whereas the imaginary parts are lower during pre-monsoon and monsoon, with monsoon values being the lowest due to a prominent reduction in aerosol content due to precipitation. Though both real and imaginary parts of RI are lower during monsoon and post-monsoon, SSA is lower during post-monsoon than monsoon (Fig. 3) owing to a prominent increase in the imaginary part of RI (Fig. 6d).

In Dushanbe, the real part of RI was in the 1.48-1.54 range and the imaginary part of RI was high in the winter (0.009) and low in summer (0.002) (Rupakheti et al., 2020). The real part of RI was higher in summer compared to winter whereas the imaginary part was higher in winter, consistent with SSA seasonal variation (low in winter due to high imaginary RI). The higher imaginary RI values indicate absorption by fine mode BC aerosols in winter (Rupakheti et al., 2020). It was noted that the aerosols in winter over Dushanbe appeared to be significantly different from other seasons in their content and composition (Rupakheti et al., 2020). Over Minsk, Belarus, the real part of RI varied between 1.46 and 1.52 during the year and the imaginary part of RI was in the 0.008-0.022 range (Filonchyk et al., 2021). The imaginary part of RI was higher than Dushanbe suggesting the dominance of anthropogenic aerosols. The imaginary part of RI in winter was the highest (≥0.20) followed by autumn, spring and summer consistent with seasonal variations in SSA. The real part of RI across the present study region is in the 1.4-1.6 range (except in New Delhi only in post-monsoon when it is lower than 1.4) and the imaginary part of RI is higher than 0.1 in post-monsoon and winter; the imaginary part of RI is the highest over new Delhi in post-monsoon (>0.2). These seasonal features and values of RI are consistent with the seasonal variations in the dominance of aerosols that are of anthropogenic origin in post-monsoon and winter and that of mixture of natural and anthropogenic origin in pre-monsoon and monsoon over the IGP and the Himalayas similar to that of Dushanbe and Minsk. This comparison reveals a commonality of aerosols between the Himalayas, IGP, Minsk and Dushanbe, while at the same time demonstrates the intra-regional variability of dominant aerosol types over the spatial domain of the IGP (western, central and eastern) up to the Himalayas.

4.2. *Aerosol type and absorbing aerosol type*

The aerosol types over the study region exhibit seasonal variations consistent with aerosol sources that are present over this region (Figs. 2–6). Based on the above metrics, the aerosol types over Pokhara and Kathmandu as well as Lumbini are of UI and BB origin only, and dust

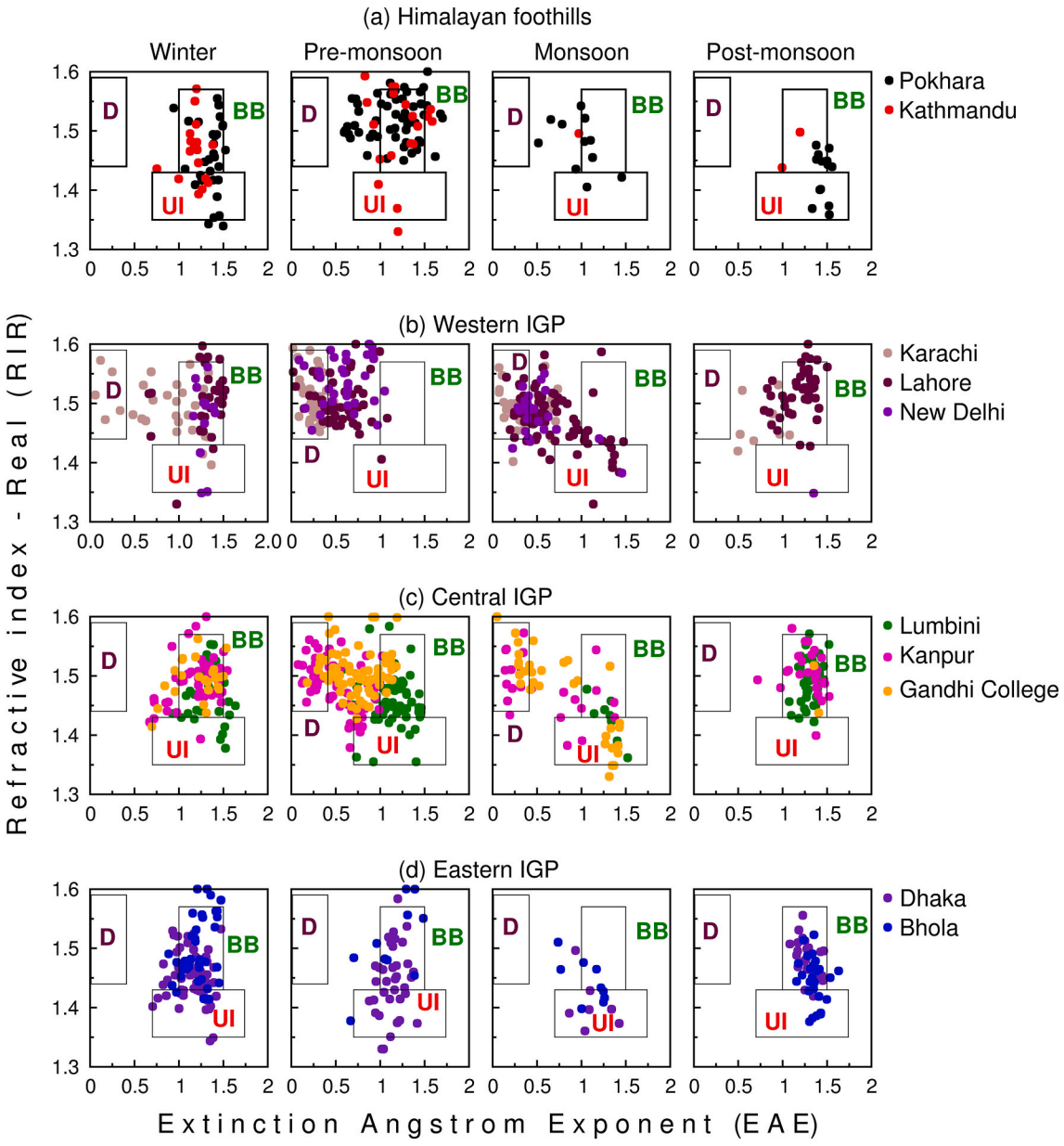

Fig. 7. Aerosol types over ten locations in – (a) Himalayan foothills, (b) western IGP, (c) central IGP and (d) eastern IGP during winter, pre-monsoon, monsoon and post-monsoon. The aerosol types are classified as dust (D), biomass burning (BB) and Urban-Industrial (UI) based on the relation between daily values of the extinction Ångström exponent (EAE) and refractive index – real part (RIR). The boxes in each figure represent bounds for the above aerosol types (Table 1).

is not present over the northern edge of central IGP and the Himalayan foothills throughout the year. Identifying and designating pure marine particles are challenging because of their high SSA (~1), coarse size, and small EAE (Russell et al., 2010, 2014), and is not important here as sea salt was found to be negligible over the Himalayan foothills (Tripathee et al., 2017). Similarly, classification of 'pure' dust is equally difficult (Russell et al., 2014), which, once again is not present over the Himalayan foothills. Dust as an aerosol type is present over Karachi and Lahore during three seasons except for the post-monsoon (Fig. 7b) which is consistent with a decreasing SSA spectra (Fig. 3b). Dust is absent over New Delhi during post-monsoon and winter. UI and BB aerosol types are present throughout the year over Karachi and Lahore, however, because of higher dust dominance the SSA spectra increases as wavelength increases during pre-monsoon and monsoon, while the SSA spectra decreases during winter (less dust) and post-monsoon (no dust). The aerosol type over New Delhi, Kanpur and Gandhi College are similar to Karachi and Lahore; dust is predominant during pre-monsoon and absent during winter and post-monsoon (Fig. 7c). Similar to the Himalayan foothills, over Dhaka and Bhola in the eastern IGP, dust is absent throughout the year (Fig. 7d). Dust transported from long-range from the arid and semi-arid regions that are west of IGP (Fig. 1), was found to exhibit a gradient in the IGP with more dust from Karachi to Kanpur and less over Gandhi College, although the spatial distance (aerial distance) between Kanpur and Gandhi College is ~500 km only (Ansari and Ramachandran, 2023). Thus, this analysis reconfirms the existence of spatial gradient in dust and associated transport across the IGP and also reveals that it is also true for the Himalayan foothills, and the amount of dust particles in the atmosphere becomes negligible as we move to east. The aerosol types identified using this approach, combined with the analysis of SSA spectra corroborate well the features observed in aerosol

chemical composition, emphasizing that a comprehensive evaluation of this sort can provide information on the chemical composition of aerosols in an unequivocal manner.

Similar to the aerosol types, the absorbing aerosol types over the Himalayan foothills (Pokhara and Kathmandu), and Lumbini are MBC and Mixed throughout the year (Fig. 8). During the winter and post-monsoon seasons the absorbing aerosol type over Himalayan foothills and central IGP are MBC (Fig. 8a–c). The mostly dust (MD) absorbing aerosol type is negligible over the Himalayan foothills (Fig. 8). This classification asserts absence of pure dust over these two regions identified earlier in aerosol typing (Fig. 7). The absorbing aerosol types obtained in the present study agree with those reported earlier (Rupakheti et al., 2019). The winter and pre-monsoon seasons in the Himalayan foothills are dominated by biomass burning emissions and BC (Rupakheti et al., 2019) as seen here; further, the long-range transport of UI aerosols (BC-dominated) from the polluted IGP are also abundant over the Himalayan foothills during winter, pre-monsoon, and post-monsoon. Over the western IGP (Karachi and Lahore), the absorbing aerosol types exhibit a distinct seasonal variation – MD is almost negligible in post-monsoon whereas MBC is almost nil during pre-monsoon (Fig. 8b) over both the locations. New Delhi follows the seasonal patterns of Karachi and Lahore during pre-monsoon (low or no MBC), monsoon (all MBC, Mixed and MD present), and post-monsoon (no MD) while its pattern is similar to Kanpur and Gandhi College during winter (no MD). Over the two central IGP sites (Kanpur and Gandhi College) all the three absorbing aerosol types are found only in monsoon, MD is completely absent in winter and post-monsoon, and MBC is negligibly small during pre-monsoon, while over Lumbini MD is absent throughout the year (Fig. 8c). The MD absorbing aerosol type is absent throughout the year over the eastern IGP (Dhaka and Bhola), and in addition Mixed is absent during post-monsoon and winter (Fig. 8). Further, over Dhaka and Bhola, the absorbing aerosol type is MBC only

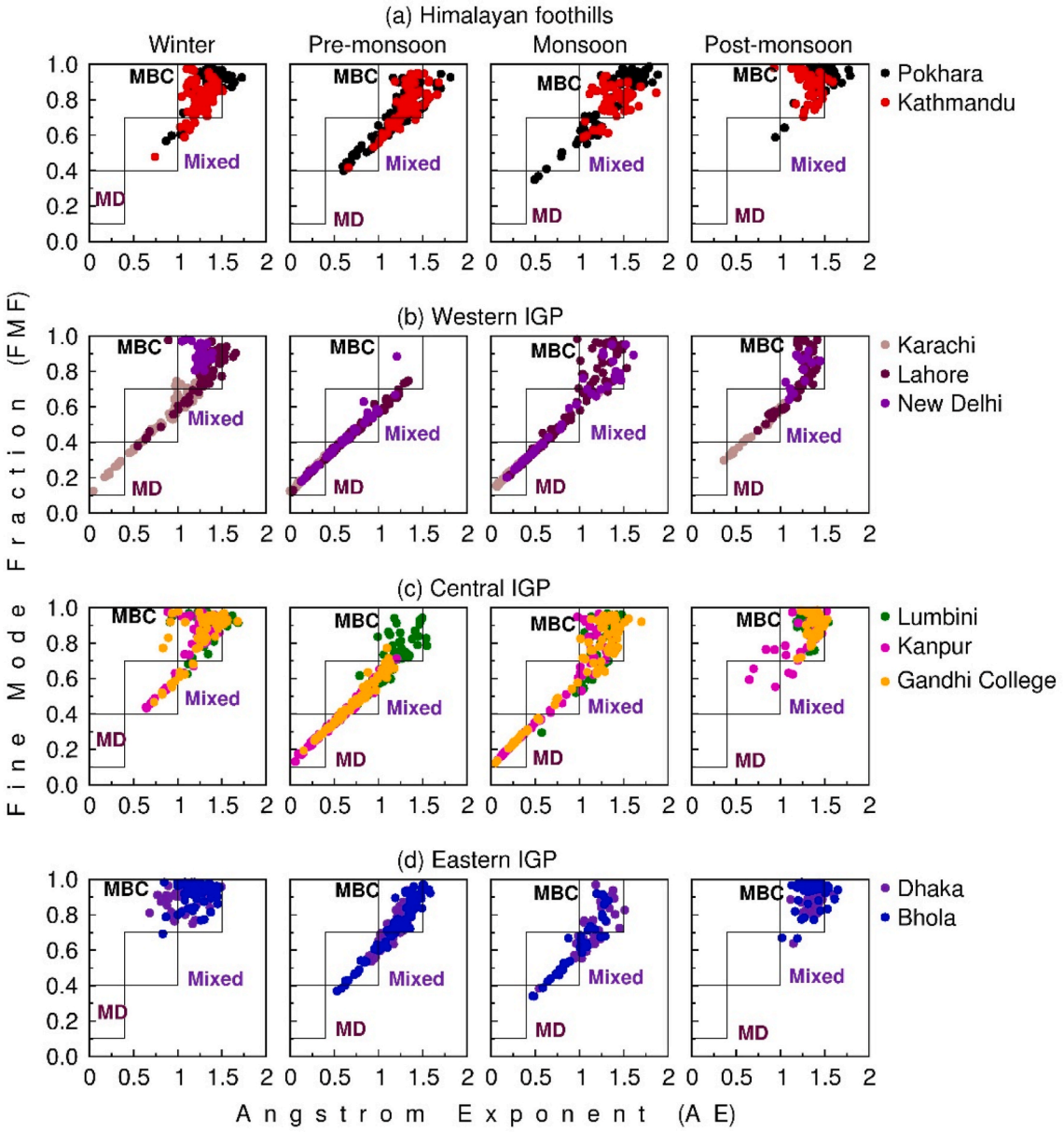

Fig. 8. Absorbing aerosol types over the ten study locations in (a) Himalayan foothills, (b) western IGP, (c) central IGP and (d) eastern IGP in winter, pre-monsoon, monsoon and post-monsoon. They are classified as Mostly BC (MBC), Mostly dust (MD) and Mixed (BC and dust). This classification is based on the daily values of Ångström exponent (AE) vs. fine mode fraction (FMF) of the aerosol optical depth (AOD). The different boxes in the figure correspond to the bounds of the three absorbing aerosol types (Table 1).

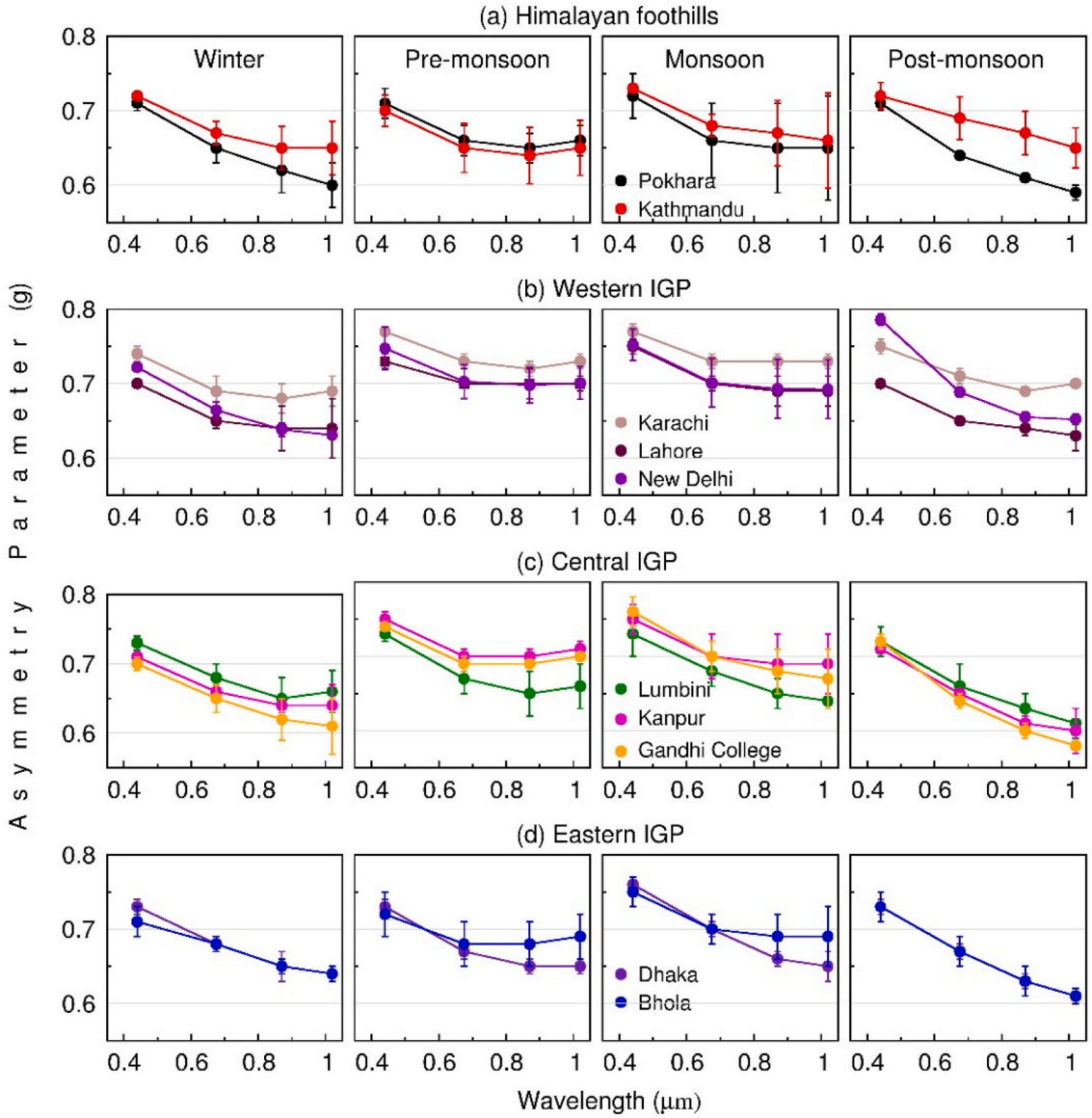

Fig. 9. Spectra of asymmetry parameter (g) in the wavelength range of 0.44-1.02 μm for different seasons over the study locations in – (a) Himalayan foothills, (b) western IGP, (c) central IGP, and (d) eastern IGP (Dhaka and Bhola in Bangladesh). Vertical bars correspond to ±1σ (standard deviation) from the respective seasonal mean values.

during post-monsoon and winter which concurs well with the lower SSA values obtained during these seasons (Fig. 3).

4.3. Asymmetry parameter (g)

The asymmetry parameter (*g*), defined as the average of the cosine of the scattering angles for scattered radiation, provides a measure of angular distribution of aerosol scattered radiation. The value of *g* depends on the size and composition of aerosols. Consequently, *g* for continental, urban/industrial and biomass burning aerosols is lower than maritime (sea salt) and dust aerosols. The *g* value is lower at 0.60 for urban/industrial aerosols, and varies between 0.61 and 0.63 for continental aerosols – clean (0.61), average (0.62) and polluted (0.63) (Hess et al., 1998). The *g* value is higher for dust (0.72) and maritime aerosols (clean (0.68) and polluted (0.65)). The asymmetry parameter decreases from maritime polluted aerosols because of the presence of black carbon aerosols, whose *g* is the lowest at 0.34 (Hess et al., 1998). All the aerosol types mentioned above will have additional components corresponding to the respective environment (e.g., coastal areas may have more sea salt particles, and urban regions near desert will be influenced by dust), and their abundances can vary which will influence their size and composition, and hence their optical and physical properties including SSA, refractive index and *g* (Hess et al., 1998). The *g* values mostly lie within 0.6-0.8 over the IGP and the Himalayan foothills, however, their spectra exhibit intra-regional and -seasonal variations. The *g* values decrease slowly as wavelength increases in winter, monsoon and post-monsoon over Pokhara and Kathmandu (Fig. 9) indicating the dominance of particles in fine mode. The *g* values decrease from 0.44 to 0.87 μm, and slightly increase at 1.02 μm during pre-monsoon over the Himalayan foothills; such a feature in *g* arises due to the abundance of absorbing aerosols (Mostly BC particles coming from UI and BB origin) as seen earlier (Figs. 7 and 8). Over Karachi and Lahore *g* values are slightly higher than the other locations and the decrease with respect to wavelength is not so significant (Fig. 9) (slight

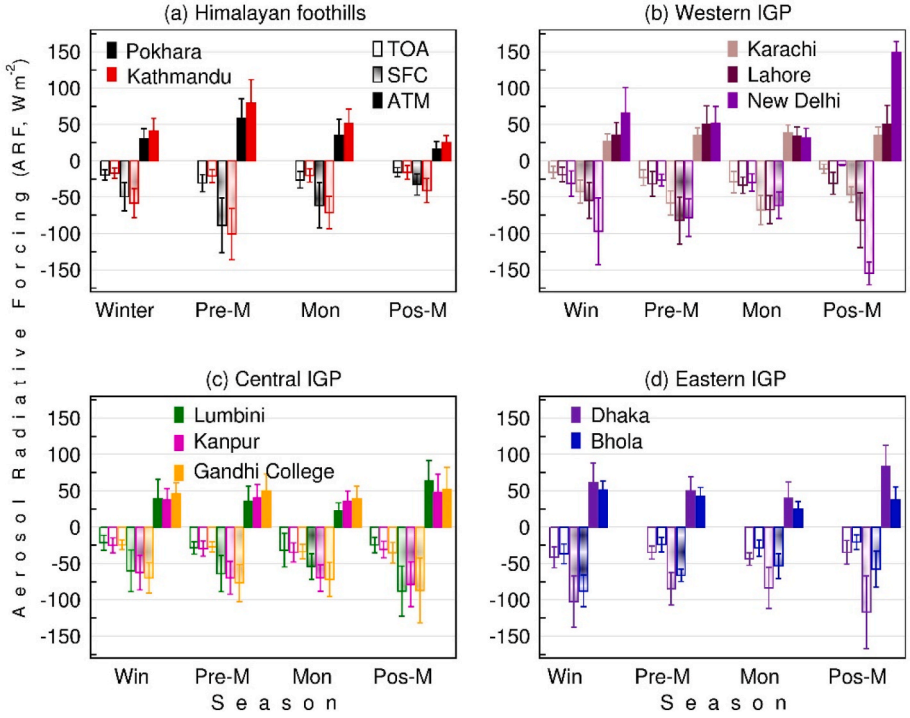

Fig. 10. Seasonal mean aerosol radiative forcing (ARF) over the study locations in the (a) Himalayan foothills, (b) Western IGP, (c) Central IGP and the (d) Eastern IGP, respectively. Open bars correspond to ARF at the top of the atmosphere (TOA), bars filled with dots correspond to ARF at the surface (SFC) and the filled bars represent the ARF in the atmosphere (ATM), respectively. Vertical bars correspond to ±1σ (standard deviation) from the mean.

spectral slope), a feature consistent with the locations dominantly influenced by dust, and mixed aerosols (BC and dust). The spectral features of *g* over New Delhi, Kanpur, Gandhi College and Lumbini are similar to that of Karachi and Lahore; *g* values are higher in pre-monsoon and monsoon when dust and sea salt particles, which are in coarse mode, dominate the aerosol size distribution. The *g* value at 0.44 μm over New Delhi during post-monsoon is the highest and the spectra of *g* is quite steeper, which occurs due to the dominant increase in the emissions of fine mode aerosols from agro-residue burning during this season. The *g* spectra over Dhaka and Bhola are steep during post-monsoon and winter when these locations are dominated by fine mode aerosols (MBC, Fig. 8), while the *g* spectrum is linear or shows a slight increase beyond 0.8 μm during pre-monsoon and monsoon due to the presence of Mixed and MBC (Fig. 8) aerosols. Thus, it is clear that *g* and its spectral dependence over the IGP and the Himalayan foothills are compatible with dominant aerosol types prevalent in this region in different seasons.

The annual mean *g* over Dushanbe was 0.69; winter *g* was the lowest at 0.63 followed by spring (0.68), autumn (0.69) and summer (0.71) (Rupakheti et al., 2020). In winter *g* values over Dushanbe decreased more rapidly between 0.44 and 0.675 μm followed by a gradual decrease thereafter, whereas in other seasons *g* decreased gradually between 0.44 and 0.675 μm followed by a slight increase or remaining more or less stable between 0.675 and 1.02 μm indicating the presence of coarse mode aerosols (Rupakheti et al., 2020). In contrast, *g* over Minsk were higher at shorter wavelengths and decreased from 0.44 to 1.02 μm wavelength range with winter values being higher due to the predominance of fine mode aerosols of anthropogenic origin (Filonchyk et al., 2021). The *g* values at 0.675 μm were higher during winter and autumn due to a greater fraction of coarse mode particles whereas the respective values were lower in spring and summer due to the predominance of fine mode aerosols (Filonchyk et al., 2021). The spectral and seasonal variations of *g* over the Himalayan foothills and the IGP are consistent with the dominant aerosol types and sizes which exhibit seasonal variations, similar to Dushanbe and Minsk. In summary, lower SSA and *g*, lower real RI and higher imaginary RI are consistent with the abundance of light absorbing fine mode aerosols (e.g., winter) whereas higher SSA and *g*, higher real RI, lower imaginary RI corroborate the dominance of dust aerosols (e.g., monsoon) over the IGP, Himalayas, Dushanbe and Minsk.

4.4. Aerosol radiative forcing, forcing efficiency, and heating rate

The ARF over the IGP and the Himalayan foothills also shows significant vertical (SFC, TOA, and ATM), intra-spatial (location to location) and intra-annual (seasonal) variations (Fig. 10). ARF at each level exhibit substantial variability with changes in AOD and SSA, and the magnitude of this variability depends on AOD and SSA values. For a higher AOD, a decrease in SSA substantially reduces the TOA forcing (less negative), enhances the SFC (more negative) and the ATM forcing (more positive). These effects on ARF become weaker for lower aerosol loading (lower AOD). The non-linear dependence of ARF_{ATM} on SSA is most pronounced when for a constant AOD, a reduction in SSA leads to a disproportionately larger increase in ATM forcing compared to the associated changes in SFC and TOA forcing. The seasonal average ARF_{TOA} over Pokhara and Kathmandu is in the −10 to −40 Wm^{-2} range during the year. The magnitude of spatial variation is different on seasonal scales, for example, ARF_{TOA} is more negative over Pokhara than Kathmandu. The ARF_{TOA} becomes more negative when SSA is higher (Fig. 10a) – SSA over Pokhara is higher than over Kathmandu throughout the year (Fig. 3a). A less negative ARF_{TOA} (due to lower SSA) and a more negative ARF_{SFC} over Kathmandu results in higher ARF_{ATM} over Kathmandu compared to Pokhara throughout the year (Fig. 10a) as mentioned above. The seasonal mean AODs (at 0.50 μm) (winter, pre-monsoon, monsoon and post-monsoon) at each location during the study period are – Pokhara (0.42, 0.76, 0.29, 0.32), Kathmandu (0.34, 0.65, 0.25, 0.31), Karachi (0.35, 0.50, 0.82, 0.31), Lahore (0.45, 0.62, 0.77, 0.68), New Delhi (0.69, 0.68, 0.59, 0.79), Lumbini (0.54, 0.67,

0.59, 0.86), Kanpur (0.72, 0.61, 0.66, 0.80), Gandhi College (0.81, 0.64, 0.60, 0.83), Dhaka (0.96, 0.79, 0.55, 0.85), and Bhola (0.83, 0.70, 0.44, 0.57) (Fig. 2), respectively.

The ARF_{ATM} is higher for lower SSA (Fig. 10) – SSA is the lowest in Kathmandu during pre-monsoon and as a result ARF_{ATM} is the highest among the three sites in Nepal in pre-monsoon. Over Karachi and Lahore, ARF_{TOA} exhibits less significant variations than ARF_{SFC}. The ARF_{SFC} increases (becomes more negative) over Karachi as the AOD increases from winter to monsoon (refer above for the seasonal mean AOD values). During post-monsoon SSA over Karachi and Lahore are comparable (Fig. 3b), however, ARF over Lahore is higher because of higher AOD (0.68). Among all the sites, ARF_{ATM} over New Delhi is the highest during post-monsoon (Fig. 10b). The ARF_{TOA} reaches its lowest value (~-5 Wm^{-2}) over New Delhi in post-monsoon from about −25 Wm^{-2} (Fig. 10b) in other seasons, consistent with the fact that as SSA decreases the ARF_{TOA} becomes less negative, and SSA in post-monsoon over New Delhi is the lowest among all the study locations (Fig. 3b). Aerosols with higher SSA (>0.95) are predominantly scatterers, and increase the amount of radiation backscattered to space resulting in a higher negative ARF_{TOA}, whereas aerosols with lower SSA absorb radiation and decrease the amount of radiation scattered back to space producing a less negative ARF_{TOA} as seen here. The ARF_{TOA}, ARF_{SFC} and ARF_{ATM} over Lumbini, Kanpur, and Gandhi College are comparable to each other owing to similar AOD (Fig. 2c), SSA (Fig. 3c) and *g* values (Fig. 9c). The winter season ARF_{SFC} is the highest over Dhaka (Fig. 10d) because of quite high AOD (~1) (Fig. 2d). The ARF_{SFC} is ≤ -50 Wm^{-2} over the entire region, and the ARF_{ATM} is ≥ 50 Wm^{-2} emphasizing that the aerosol-induced surface cooling and atmospheric warming are regionally coherent, uniform, and significant over this large regional domain throughout the year. In comparison, the ARF_{ATM} for biomass burning aerosols from peninsular Southeast Asia, a biomass-burning hotspot, was found to be 5-10 Wm^{-2} over the source area which increased to 10-20 Wm^{-2} over the downwind area (Dong et al., 2019). The ARF_{ATM} obtained in the current study over South Asia is significantly higher (at least by 2-5 times) than ARF_{ATM} due to biomass burning aerosols from Southeast Asia.

The ARFE (= ARF normalized by the AOD (Wm^{-2} AOD^{-1})), is a functional metric to assess the effect of scattering and absorbing aerosols, besides SSA, through which the influence of AOD on ARF is excluded. The ARFE values are higher than ARF (Fig. 11). The $ARFE_{SFC}$ and $ARFE_{ATM}$ vary more significantly on seasonal and spatial scales than $ARFE_{TOA}$. The $ARFE_{SFC}$ and $ARFE_{ATM}$ closely follow the SSA (Fig. 3). At the outset, the ARFE is highest for Kathmandu (Fig. 11) across the entire IGP and the Himalayan foothills (except during the post-monsoon over New Delhi), and the values increase gradually from Lumbini (lower elevation) to Kathmandu (higher elevation), with Pokhara values lying in between. The $ARFE_{ATM}$ over New Delhi during post-monsoon is the highest because of the lowest SSA (Fig. 3c). The seasonal variations in ARFE differ (Fig. 11) as compared to ARF (Fig. 10) as ARFE is normalized with AOD (Fig. 2). These results clearly indicate that for the same ARF, ARFE will be higher for lower SSA (i.e. with higher proportion of absorbing aerosols). These high ARFE values at all altitudes indicate that aerosols efficiently regulate the incoming solar flux over the entire region in all seasons.

Aerosols exhibit significant altitudinal variations as well. For example, in the troposphere, they exhibit a large gradient from the surface to up to 5-10 km, and this gradient is dependent on regions, seasons, transport patterns and winds (e.g., Gui et al., 2021). The globally gridded aerosol extinction data from the Cloud-Aerosol Lidar with Orthogonal Polarization (CALIOP) onboard CALIPSO Level-3 aerosol profile product based on monthly statistics, where all Level-2 aerosol profiles within each month are reported separately at a near-global scale on a uniform 2.0° × 5.0° (latitude × longitude) (Gui et al., 2021) for 2012-2015 are utilized to determine the upper bound altitude from the elevation (surface) of each location up to which aerosols contribute the maximum to aerosol extinction. This analysis is performed as assuming a constant upper bound of a particular value (say 5 or 10 km) precludes that aerosols are vertically uniformly distributed throughout the layer and would lead to a lower heating rate when everything else remains constant. This becomes important over a region

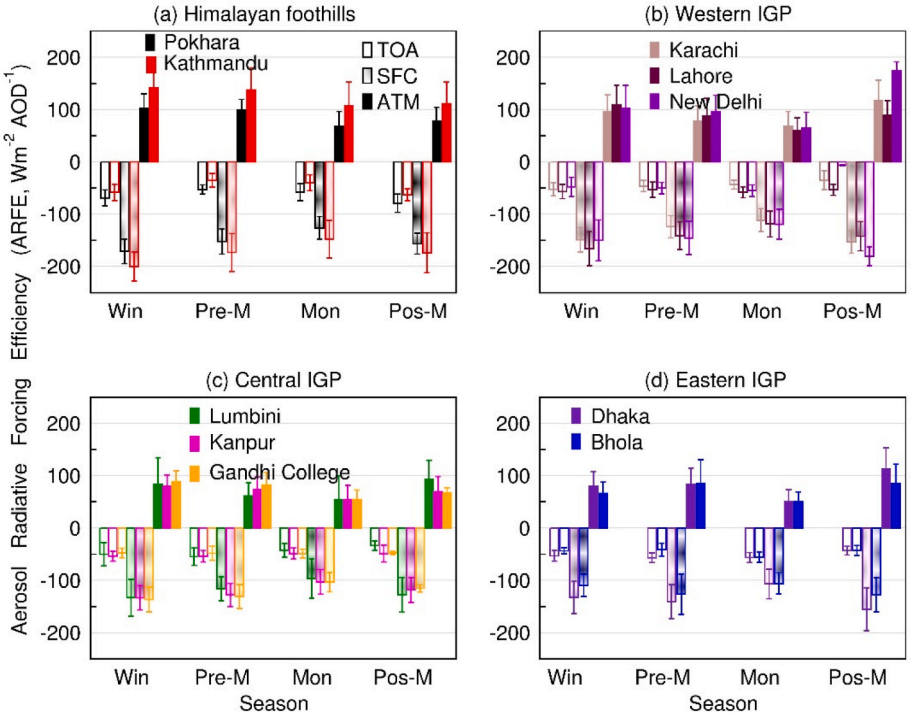

Fig. 11. Seasonal mean aerosol radiative forcing efficiency (ARFE = ARF/AOD) over the study locations in the (a) Himalayan foothills, (b) Western IGP, (c) Central IGP and the (d) Eastern IGP, respectively. Open bars correspond to ARFE at the top of the atmosphere (TOA), bars filled with dots correspond to ARFE at the surface (SFC) and the filled bars represent the ARFE in the atmosphere (ATM), respectively. Vertical bars correspond to ±1σ (standard deviation) from the mean.

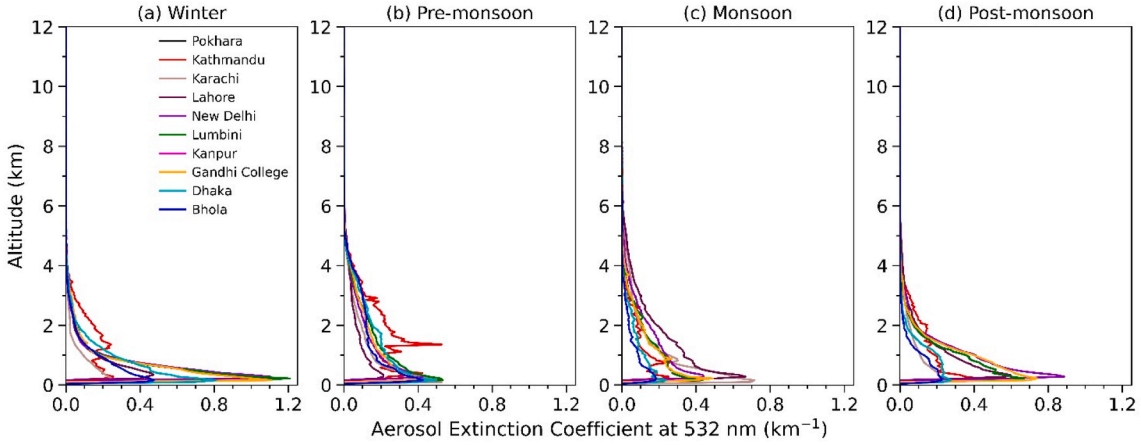

Fig. 12. Seasonal mean aerosol extinction coefficient profiles at 532 nm (km^{-1}) obtained from CALIPSO for the study locations during (a) winter, (b) pre-monsoon, (c) monsoon and (d) post-monsoon.

such as the IGP and the Himalayas where the aerosols are distributed non-uniformly and exhibit structures (such as higher concentration near the surface and elevated layer at 3-4 km are often observed) as a function of altitude (Fig. 12). The aerosol extinction profiles are plotted up to 12 km because the tropospheric aerosol content above this altitude was found to contribute <0.05%, to columnar aerosol extinction which is negligible (Gui et al., 2021 and references therein). The aerosol extinction profiles show distinct seasonal and spatial differences across the IGP and the Himalayas. The aerosol extinction is higher in the lower altitudes (<4 km) during winter and post-monsoon whereas the vertical extent of aerosols increases during pre-monsoon and monsoon (Fig. 12). Aerosol extinction up to 1 km is higher in winter and post-monsoon as compared to pre-monsoon and monsoon over this region (Fig. 12). During pre-monsoon aerosol extinction above 1 km is higher, exhibits a peak around 1.5 km, and is comparable to the extinction near surface supporting quite well the higher AOD over Kathmandu in this season (Fig. 2a). The aerosol extinction over Kathmandu is higher than all the other study locations up to 4 km during pre-monsoon giving rise to an elevated aerosol layer consistent with the prevalent meteorology (convection, updraft, and mountain valley winds) over the complex topographical conditions of the Himalayas. The seasonal mean upper bound altitude up to which aerosols contribute 99.5% to columnar extinction at each location in the IGP and the Himalayas are estimated (Table 3) and used in the estimate of aerosol-induced atmospheric heating rate (eqn. (1)). The upper bound altitudes vary, and exhibit distinct regional and seasonal variations - differing by about a 1 km or so in a season among the study locations, and differing by ~2 km over a particular location during the year. The upper bound altitudes are lower in winter and

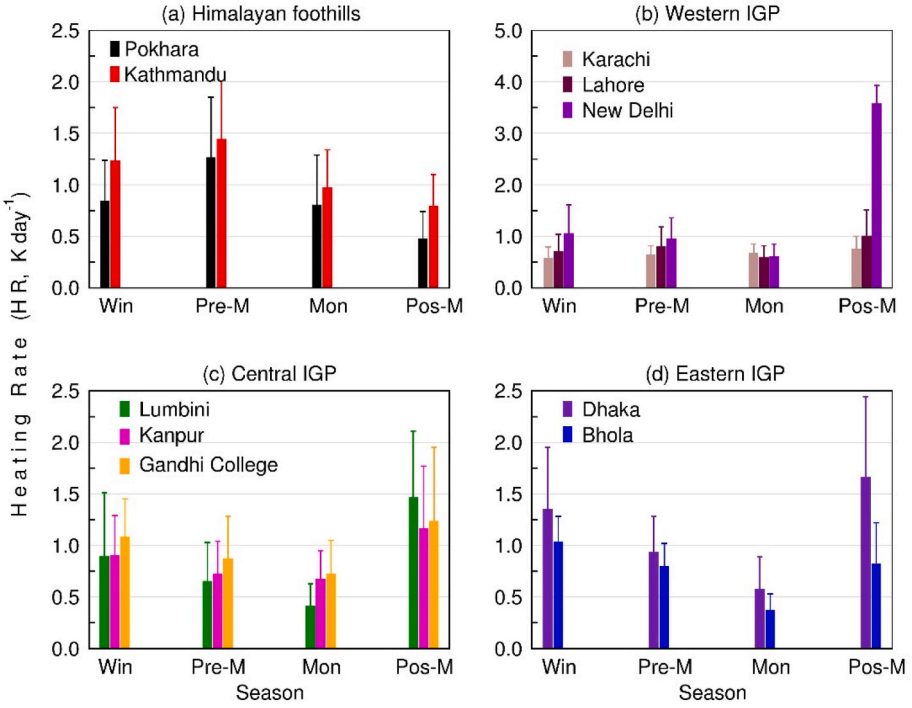

Fig. 13. Seasonal mean aerosol-induced atmospheric solar heating rate (HR, Kelvin (K) day^{-1}) over the study locations in the (a) Himalayan foothills, (b) Western IGP, (c) Central IGP and the (d) Eastern IGP, respectively. Note the scale of axis of ordinates (y-axis) in (b) is twice that of (a), (c) and (d). Vertical bars correspond to ±1σ (standard deviation) from the mean.

post-monsoon than pre-monsoon and monsoon as the shallower planetary boundary layers during post-monsoon and winter tend to confine aerosols near the surface (Table 3).

The atmospheric solar heating rate (HR) induced by aerosols is now a function of AOD, SSA, *g* and the upper bound altitude (Table 3). The HR is $\geq$ 0.4 K day^{-1} across the IGP and the Himalayas throughout the year (Fig. 13), and exhibit significant seasonal and spatial variations. The HR is the highest over Kathmandu (~1.5 K day^{-1}) during pre-monsoon consistent with lower SSA (Fig. 3) and high ARF_{ATM} (Fig. 10). During post-monsoon the HR is higher over Lumbini in central IGP than Kathmandu in the Himalayan foothills. The HR varies between 0.5 and 1.0 K day^{-1} over Karachi and Lahore during the year; Lahore HR is higher during winter, pre-monsoon and post-monsoon whereas in monsoon the Karachi HR is slightly higher (Fig. 13). An HR of ~4 K day^{-1} HR over New Delhi during post-monsoon, which is the highest among all sites (Fig. 13), arises due very low SSA values (Fig. 3b) and high AOD (Fig. 2b). The HR decreases gradually from winter to monsoon over Dhaka and Bhola, the monsoon values being the lowest, and increasing again during post-monsoon (Fig. 13). The HR and ARF_{ATM} over Bhola during the year are lower than Dhaka. SSA and AAOD over Dhaka and Bhola are comparable except in post-monsoon, when SSA is higher (Fig. 3) and AAOD is lower (Fig. 4) in Bhola than Dhaka. The ARF_{ATM} and HR over Dhaka and Bhola differ significantly during post-monsoon with Dhaka values being higher which occurs due to a significantly higher AOD (0.85) and lower SSA (Fig. 3) over Dhaka compared to Bhola (AOD = 0.57) (Fig. 2). The pre-monsoon HR of $\geq$1.0 K day^{-1} over Pokhara and Kathmandu is higher than those reported earlier, which were in the range of 0.45-0.7 K day^{-1} during pre-monsoon (March 2006) over the Indian Ocean (Ramanathan et al., 2007), and were attributed to the atmospheric brown cloud. Higher ARFE and aerosol-induced heating rate on a regional scale reported here when compared to previous studies indicate that the previously reported HR values may not be depicting a regional-mean scenario appropriately.

The seasonal average ARF_{ATM} was in the 20 (spring) – 37 (winter) Wm^{-2} range over Dushanbe (Rupakheti et al., 2020). The ARF_{ATM} values were found to be lower than that of urban atmosphere. The ARF did not exhibit significant seasonal variability (Rupakheti et al., 2020). The seasonal average ARF_{ATM} was lower over Minsk and was between 14 and 23 Wm^{-2} (Filonchyk et al., 2021). In comparison, the ARF_{ATM} values over the IGP and the Himalayan foothills generally are higher than those obtained over Dushanbe and Minsk (Fig. 10). The $ARFE_{ATM}$ over Dushanbe was in the 120 (lowest in autumn, AOD = 0.30) - 150 (highest in winter, AOD = 0.23) Wm^{-2} AOD^{-1} range (Rupakheti et al., 2020), clearly emphasizing the role of SSA in influencing the ARF as SSA was the lower in winter (0.90) compared to autumn (0.93). In Minsk, $ARFE_{ATM}$ varied between 96 (summer) and 159 (winter) Wm^{-2} AOD^{-1} (Filonchyk et al., 2021). AOD and SSA in winter over Minsk were 0.18 and 0.89, respectively, whereas during summer AOD and SSA were 0.23 and 0.93, respectively. Since, SSA-ARF relation is non-linear, a small difference in SSA can result in a large difference in ARFE as seen here. The ARFE over the IGP and the Himalayan foothills is comparable to that of Dushanbe and Minsk despite significantly higher AODs than that of Dushanbe and Minsk mainly because of lower SSA at the IGP and Himalayan sites (Figs. 3 and 11). The HR over Dushanbe (calculated with the upper bound altitude set to 3 km) ranges from 0.9 to 1.5 K day^{-1} during the year, while over Minsk HR it ranges from 0.40 to 0.64 K day^{-1}. The HR over Dushanbe (and Minsk too) is comparable to (lower than) that over the IGP and the Himalayan foothills. HR is ~1.5 K day^{-1} over Kathmandu (pre-monsoon) and New Delhi (post-monsoon) (Fig. 13) as a result of high AOD (Fig. 2) and low SSA (Fig. 3), confirming that the study region is highly polluted.

HR can decrease or vary significantly with an increase or changes in the upper altitude bound. To illustrate further, for example, for an ARF_{ATM} value of 50 Wm^{-2}, the HR (eqn. (1)) is estimated to be 1.4 K day^{-1} for upper bound 3 km asl ($\Delta P = 298$ hPa), 0.9 K day^{-1} for 5 km asl ($\Delta P = 454$ hPa), and 0.6 K day^{-1} for 10 km asl ($\Delta P = 727$ hPa), respectively. The HR calculated with 3 km asl as the upper bound is ca. 36% and 60% higher than the HR obtained using 5 km asl and 10 km asl, respectively. Furthermore, HR of the column using 5 km asl is 33% higher than that with 10 km asl top of the column. Thus, the differences in HR, between the IGP and the Himalayas, and Dushanbe and Minsk arise from differences in AOD, SSA, *g* and the upper bound altitudes of atmosphere (which vary seasonally in this study over the IGP and the Himalayas (Table 3), compared to a constant upper bound of 3 km over Dushanbe and Minsk).

The ratio R_{ST} (=ARF_{SFC}/ARF_{TOA}) is estimated to determine whether scattering and/or absorbing aerosols are dominantly present in the atmosphere, with $R_{ST}<2$ suggesting the presence of scattering aerosols and $R_{ST}>3$ indicating the presence of absorbing aerosols in the atmosphere (Rupakheti et al., 2020). The annual average R_{ST} was 3.66 over Dushanbe, and R_{ST} in all the seasons was >3 indicating the dominant presence of absorbing aerosols throughout the year over Dushanbe (Rupakheti et al., 2020). In Minsk, the annual average R_{ST} (calculated from ARF_{SFC} and ARF_{TOA} given in Filonchyk et al., 2021) was close to 3. However, R_{ST} showed significant seasonal variations, varying from a low of 2.19 (monsoon) to a high of 4.93 (winter) indicating the dominance of scattering aerosols in monsoon as compared to winter which was dominated by absorbing aerosols consistent with RI and SSA. The annual mean R_{ST} is 2.46 (Pokhara), 3.59 (Kathmandu), 2.92 (Karachi), 2.53 (Lahore), 9.11 (New Delhi), 2.59 (Lumbini), 2.35 (Kanpur), 2.59 (Gandhi College), 2.55 (Dhaka) and 2.46 (Bhola), respectively, over the study region; these R_{ST} values confirm the presence of scattering and absorbing aerosols in this region with a higher abundance of absorbing aerosols (Fig. 10). The ratio is ~5.0 over Kathmandu in pre-monsoon corroborating the low SSA (0.8) and in New Delhi >5 in post-monsoon when SSA is the lowest ($\leq$0.8) (Fig. 3). The monsoon R_{ST} is close to 2 (2.19) across the entire study region suggesting the dominance of scattering aerosols, (due to wet removal (rainfall) and hygroscopic growth (higher RH)), whereas during the other three seasons the regional average R_{ST} is nearly 3 (value lies between 2.76 and 2.97) indicating the dominance of absorbing aerosols in the atmosphere consistent with the seasonal features in SSA, AAOD, and RI.

5. Discussion and implications

The uncertainty in aerosol radiative forcing continues to impede the attribution of changes due to aerosols in the climate system, including on temperature (IPCC et al., 2021). A major part of the uncertainty in ARF arises from the uncertainty in SSA and AAOD. The AOD and ARF are linearly related; for the same SSA, if AOD increases by 10% then the ARF will increase by the same amount, whereas when SSA decreases by 10% from 0.90 then the ARF increases by ~25%, thus making the relation between SSA and ARF non-linear (Ramachandran et al., 2020). This non-linearity between ARF and SSA precisely arises because of the variations in ARF_{TOA} (as explained earlier). In addition, any changes in the asymmetry parameter (*g*) contributes negligibly to ARF variations, thus, for more accurate estimates of ARF, an accurate determination of SSA is more crucial than AOD and *g*. It is rather more challenging to measure AAOD, spectral absorption and SSA accurately from space, as AAOD and SSA retrieved from the Ozone Monitoring Instrument (OMI) measurements are reported to exhibit significant biases (Shindell et al., 2013; Jethva et al., 2014).

Global and regional models tend to significantly underestimate the BC mass concentrations and aerosol absorption over South Asia including the IGP and the Himalayas (IPCC et al., 2021; Jimenez et al., 2009; Shindell et al., 2013). The Atmospheric Chemistry and Climate Model Intercomparison Project (ACCMIP) reported that models strongly underestimate AAOD in many regions, and the spatial correlations

between model simulated AAOD and OMI retrieved AAOD were reported poor (Shindell et al., 2013). The SSA simulated by global model/chemistry transport models (GOCART and MOZART) over the IGP was higher because the simulated BC mass concentrations were quite low as mentioned earlier, and the SSA values were also seasonally invariant (Lawrence and Lelieveld, 2010). In this context, the results obtained in the present study on SSA, AAOD and radiative effects and their seasonal variations over a large spatial domain covering the IGP and the Himalayan foothills from high-quality in situ ground-based columnar observations are crucial to reduce the uncertainty in ARF estimates. The ARFE values obtained in the present study from observations over the Himalayas are significantly higher than those obtained over the Indian Ocean (Ramanathan et al., 2007), Beijing (China), and Gosan (S. Korea) (Cho et al., 2017). It is worth emphasizing that the earlier ARFE values estimated using models (Cho et al., 2017) were grossly underestimated over this South Asian region. The differences in ARF between observations and model can arise primarily only due to the differences in aerosol properties (mainly AOD and SSA), as differences in sun angles have only a very minor effect. For example, the global mean AAOD and SSA (at 0.55 μm) from the AeroCom Phase-II 16-model ensemble mean were reported to be 0.0015 and 0.95 respectively (Myhre et al., 2013) which are significantly lower (for AAOD) and higher (for SSA) than the respective values obtained over the IGP and the Himalayas.

Our results reveal that as the elevation increases in the Himalayan foothills the aerosol-induced atmospheric solar heating rates and likely the local warming (aersols plus greenhouse gases) increase. Such significantly high ARFE and HRs over the Himalayas have significant climate implications. The glaciers in the Hindu Kush-Himalayan-Tibetan Plateau region that tend to the Yangtze, the Indus and the Ganges, the major rivers in Asia have witnessed a notable retreat (Thompson et al., 2003). The atmospheric warming tendency increases with increase in elevation over this region similar to that of aerosol-induced atmospheric warming (Krishnan et al., 2019). The atmospheric warming by BC is expected to accelerate glacier and snow melt (Ramanathan et al., 2007). Our results corroborate Maurer et al. (2019) who found that the consistent ice loss observed along the entire 2000-km transect of the Himalayas could dominantly be due to a regionally coherent climate forcing attributable to the direct heating of the atmosphere by absorbing aerosols. Our quantitative results on aerosol chemical composition including spectral absorption and atmospheric heating over a region with significant uncertainty in model simulations of climate and monsoon responses are crucial to improve the assessment of radiative and climate impact aerosols including on the cryosphere and monsoon.

6. Conclusions

Quantitative knowledge on chemical and radiative properties of aerosols, including their variation across season and elevations, are still lacking and uncertain, in particular over heavily polluted source regions such as the Ingo-Gangetic Plain (IGP) and the downwind regions such as the Himalayas that receive the pollution outflow, as they still remain poorly sampled/observed. Our comprehensive regional and seasonal analysis, for the first time, of high-quality columnar aerosol observations at ten locations across the IGP and the Himalayan foothills (Karachi, Lahore and New Delhi in western IGP; Kanpur, Gandhi College and Lumbini in central IGP; Dhaka and Bhola in eastern IGP; and Pokhara and Kathmandu in the Himalayan foothills), reveals that chemical characteristics of aerosols (aerosol absorption and single scattering albedo (SSA)), aerosol- and absorbing-aerosol types, aerosol radiative effects (aerosol radiative forcing (ARF), aerosol radiative forcing efficiency (ARFE), and aerosol-induced atmospheric heating rate (HR)) vary both qualitatively and quantitatively across the IGP and the Himalayas. Aerosol optical depth (AOD) in the 0.44-1.02 μm wavelength region is $\geq$ 0.3 over all the locations the entire year, confirming that the entire region is heavily polluted, and exhibit significant spectral and seasonal variations. AODs over Pokhara and Kathmandu are highest in pre-monsoon, whereas Lumbini in Nepal has the highest AOD in post-monsoon. Karachi AE values are the lowest in the entire IGP confirming the dominance of coarse mode particles throughout the year. The Ångström Exponent (AE, slope of spectral distribution of AODs with respect wavelength and an indicator of aerosol size) values are in general higher during winter and post-monsoon due to the dominance of fine mode aerosols. Higher than 1 AE values over Pokhara, Kathmandu and Lumbini throughout the year confirm the dominance of fine mode aerosols up to the northern edge of IGP and the Himalayas. SSA and its spectral variation with wavelength confirm the significant contribution of dust to aerosol composition and absorption over the western IGP, while carbonaceous aerosols dominate the aerosol absorption in eastern IGP and Himalayas, with the central IGP falling in between. The seasonal average Absorption Ångström Exponent (AAE) values are in the range of 1 to 2 over the IGP and the Himalayas, with lower (higher) values when carbonaceous (dust) aerosols influence the sites. The AAE <1.5 over Pokhara and Kathmandu, and close to 1 over Dhaka and Bhola suggest that BC dominates the aerosol absorption throughout the year over the Himalayan foothills and eastern IGP. Furthermore, the aerosol types have an urban/industrial and biomass burning origin over Nepal as well as over Bangladesh, and dust is absent over the Himalayan foothills throughout the year. Dust is present over western and central IGP almost throughout the year except for post-monsoon. The absence of dust reveals a spatial gradient in dust and associated transport across the IGP, the Himalayan foothills and the east.

The ARF over the IGP and the Himalayan foothills shows significant variations vertically (surface, top of the atmosphere, and atmosphere), across (location) and from season to season. The seasonal average ARF_{TOA} varies between −10 and −40 Wm^{-2} over highland locations (Pokhara and Kathmandu) in the Himalayan foothills. The ARF_{TOA}, ARF_{SFC} and ARF_{ATM} over Lumbini, Kanpur, and Gandhi College are comparable during the year because of similar AOD, SSA and *g* values. The $ARF_{SFC} \leq$ -50 Wm^{-2} and $ARF_{ATM} \geq$50 Wm^{-2} due to aerosols give rise to a significant surface cooling and atmospheric warming, respectively, across the entire region. The $ARFE_{SFC}$ and $ARFE_{TOA}$ are highest for Kathmandu across the entire IGP and the Himalayas (except during post-monsoon over New Delhi). The heating rate (HR) is $\geq$ 0.4 K day^{-1} at all sites throughout the year over the IGP and the Himalayas, indicating that warming due to aerosols is quite coherent over a large region in northern South Asia. The HR $\geq$ 1.0 K day^{-1} over Pokhara and Kathmandu during pre-monsoon is significantly higher than the earlier reported HR over South Asia. The present study reveals that aerosols are efficiently cutting down the amount of solar energy reaching the Earth's surface (cooling the surface) while warming the atmosphere significantly across the IGP and the Himalayan foothills, confirming that aerosols are a major driver of climate change in the region. In the present day scenario, the regionally-coherent large aerosol-induced atmospheric heating rates could be critical to the total atmospheric warming (greenhouse plus aerosols) in the region. The quantitative knowledge of the present analysis, especially the spectral characteristics of AOD, SSA and *g*, and their seasonal variations, provides an observational basis for validating and constraining model simulations for better and more accurate simulation of spectral characteristics of aerosols and their radiative and climate impacts, over an ecologically sensitive and climatically vulnerable region.

CRediT authorship contribution statement

S. Ramachandran: Conceptualization, Data curation, Formal analysis, Investigation, Methodology, Validation, Visualization, Writing – original draft, Writing – review & editing. **Maheswar Rupakheti:** Conceptualization, Writing – review & editing.

Author information

The authors declare no competing financial interests.

Funding

This research is supported by the Research Institute for Sustainability at GFZ Helmholtz Centre for Geosciences, Potsdam, Germany (RIFS), formerly Institute for Advanced Sustainability Studies (IASS) which is funded by the German Federal Ministry of Research, Technology, and Space (BMFTR) and the Brandenburg State Ministry for Science, Research and Culture (MWFK). This work was performed when S. Ramachandran was a Senior Fellow at IASS on a sabbatical from Physical Research Laboratory, India. He is currently an Affiliate Scholar of RIFS. Physical Research Laboratory is supported by Department of Space, Government of India.

Declaration of competing interest

The authors declare that they have no known competing financial interests or personal relationships that could have appeared to influence the work reported in this paper.

Acknowledgments

We thank the principal investigators for their efforts in establishing and maintaining the AERONET sites (https://aeronet.gsfc.nasa.gov/) from which data are used in the study. Maheswar Rupakheti acknowledges Brent N. Holben from the NASA AERONET for providing two sets of CIMEL Sun-photometers for setting up AERONET sites at Bode (Kathmandu Valley) and Lumbini. We thank Dr. Kamran Ansari for downloading and plotting aerosol extinction profiles from CALIPSO (Fig. 12).

Data availability

All data used in the manuscript are available at https://aeronet.gsfc.nasa.gov/and https://doi.org/10.5067/CALIOP/CALIPSO/CAL_LID_L3_Tropospheric_APro_AllSky-Standard-V4-20.

References

Ansari, K., Ramachandran, S., 2023. Aerosol characteristics over indo-gangetic plain from ground-based AERONET and MERRA-2/CAMS model simulations. Atmos. Environ. 293, 119434. https://doi.org/10.1016/j.atmosenv.2022.119434.

Bhardwaj, P., Naja, M., Rupakheti, M., Lupascu, A., Mues, A., Panday, A.K., Kumar, R., Mahata, K.S., Lal, S., Chandola, H.C., Lawrence, M.G., 2018. Variations in surface ozone and carbon monoxide in the kathmandu valley and surrounding broader regions during SusKat-ABC field campaign: role of local and regional sources. Atmos. Chem. Phys. 18, 11949–11971. https://doi.org/10.5194/acp-18-11949-2018.

Chen, P.F., Kang, S.C., Tripathee, L., Ram, K., Rupakheti, M., Panday, A.K., Zhang, Q.G., Guo, J.M., Wang, X.X., Pu, T., Li, C.L., 2019. Light absorption properties of elemental carbon (EC) and water-soluble brown carbon (WS-BrC) in the kathmandu valley, Nepal: a 5−year study. Environ. Pollut. 261, 114239. https://doi.org/10.1016/j.envpol.2020.114239.

Cho, C., Kim, S.-W., Rupakheti, M., Park, J.-S., Panday, A., Yoon, S.-C., Kim, J.-H., Kim, H., Jeon, H., Sung, M., Kim, B.M., Hong, S.K., Park, R.J., Rupakheti, D., Mahata, K.S., Praveen, P.S., Lawrence, M.G., Holben, B., 2017. Wintertime aerosol optical and radiative properties in the kathmandu valley during the SusKat-ABC field campaign. Atmos. Chem. Phys. 17, 12617–12632. https://doi.org/10.5194/acp-17-12617-2017.

Decesari, S., Facchini, M.C., Carbone, C., Giulianelli, L., Rinaldi, M., Finessi, E., Fuzzi, S., Marinoni, A., Cristofanelli, P., Duchi, R., Bonasoni, P., Vuillermoz, E., Cozic, J., Jaffrezo, J.L., Laj, P., 2010. Chemical composition of PM_{10} and PM_1 at the high-altitude himalayan station nepal climate observatory-pyramid (NCO-P) (5079 m a.s.l.). Atmos. Chem. Phys. 10, 4583–4596. https://doi.org/10.5194/acp-10-4583-2010.

Dong, X., Fu, J.S., Huang, K., Zhu, Q., Tipton, M., 2019. Regional climate effects of biomass burning and dust in east Asia: evidence from modeling and observation. Geophys. Res. Lett. 46 (11). https://doi.org/10.1029/2019GL083984, 490-11,499.

Dubovik, O., Smirnov, A., Holben, B.N., King, M.D., Kaufman, Y.J., Eck, T.F., Schuster, I., 2000. Accuracy assessments of aerosol optical properties retrieved from aerosol robotic network (AERONET) sun and sky radiance measurements. J. Geophys. Res. 105, 9791–9806.

Dubovik, O., Holben, B., Eck, T.F., Smirnov, A., Kaufman, Y.J., King, M.D., Tanre, D., Slutsker, I., 2002. Variability of absorption and optical properties of key aerosol types observed in worldwide locations. J. Atmos. Sci. 59, 590–608.

Eck, T.F., Holben, B.N., Dubovik, O., Smirnov, A., Goloub, P., Chen, H.B., Chatenet, B., Gomes, L., Zhang, X.-Y., Tsay, S.-C., Giles, D., Slutsker, I., 2005. Columnar aerosol optical properties at AERONET sites in central eastern Asia and aerosol transport to the tropical mid-Pacific. J. Geophys. Res. 110, D06202. https://doi.org/10.1029/2004JD005274.

Filonchyk, M., Peterson, M., Yan, H., Yang, S., Chaikovsky, A., 2021. Columnar optical characteristics and radiative properties of aerosols of the AERONET site in minsk, Belarus. Atmos. Environ. 249, 118237. https://doi.org/10.1016/j.atmosenv.2021.118237.

Forster, P., Storelvmo, T., Armour, K., Collins, W., Dufresne, J.-L., Frame, D., Lunt, D.J., Mauritsen, T., Palmer, M.D., Watanabe, M., Wild, M., Zhang, H., 2021. The earth's energy budget, climate feedbacks, and climate sensitivity. In: Masson-Delmotte, V., Zhai, P., Pirani, A., Connors, S.L., Péan, C., Berger, S., Caud, N., Chen, Y., Goldfarb, L., Gomis, M.I., Huang, M., Leitzell, K., Lonnoy, E., Matthews, J.B.R., Maycock, T.K., Waterfield, T., Yelekçi, O., Yu, R., Zhou, B. (Eds.), Climate Change 2021: the Physical Science Basis. Contribution of Working Group I to the Sixth Assessment Report of the Intergovernmental Panel on Climate Change. Cambridge University Press, Cambridge, United Kingdom and New York, NY, USA, pp. 923–1054. https://doi.org/10.1017/9781009157896.009.

García, O.E., Díaz, J.P., Expósito, F.J., Díaz, A.M., Dubovik, O., Derimian, Y., Dubuisson, P., Roger, J.-C., 2012. Shortwave radiative forcing and efficiency of key aerosol types using AERONET data. Atmos. Chem. Phys. 12, 5129–5145. https://doi.org/10.5194/acp-12-5129-2012.

Gautam, R., Hsu, N.C., Tsay, S.C., Lau, K.M., Holben, B., Bell, S., Smirnov, A., Li, C., Hansell, R., Ji, Q., Payra, S., Aryal, D., Kayastha, R., Kim, K.M., 2011. Accumulation of aerosols over the indo-gangetic plains and southern slopes of the himalayas: distribution, properties and radiative effects during the 2009 pre-monsoon season. Atmos. Chem. Phys. 11, 12841–12863. https://doi.org/10.5194/acp-11-12841-2011.

Giles, D.M., Holben, B.N., Eck, T.F., Sinyuk, A., Smirnov, A., Slutsker, I., Dickerson, R.R., Thompson, A.M., Schafer, J.J., 2012. An analysis of AERONET aerosol absorption properties and classifications representative of aerosol source regions. J. Geophys. Res. 117, D17203. https://doi.org/10.1029/2012JD018127.

Giles, D.M., Sinyuk, A., Sorokin, M.G., Schafer, J.S., Smirnov, A., Slutsker, I., Eck, T.F., Holben, B.N., Lewis, J.R., Campbell, J.R., Welton, E.J., Korkin, S.V., Lyapustin, A.I., 2019. Advancements in the Aerosol Robotic Network (AERONET) Version 3 database - Automated near-real-time quality control algorithm with improved cloud screening for Sun photometer aerosol optical depth (AOD) measurements. Atmos. Meas. Tech. 12, 169–209. https://doi.org/10.5194/amt-12-169-2019.

Gui, K., Che, H., Zheng, Y., Zhao, H., Yao, W., Li, L., Zhang, L., Wang, H., Wang, Y., Zhang, X., 2021. Three-dimensional climatology, trends, and meteorological drivers of global and regional tropospheric type-dependent aerosols: insights from 13 years (2007-2019) of CALIOP observations. Atmos. Chem. Phys. 21, 15309–15336. https://doi.org/10.5194/acp-21-15309-2021.

Gustafsson, Ö., Krusa, M., Zencak, Z., Sheesley, R.J., Granat, L., Engström, E., Praveen, P.S., Rao, P.S.P., Leck, C., Rodhe, H., 2009. Brown clouds over south Asia: biomass or fossil fuel combustion. Science 323, 495–498.

Hess, M., Koepke, P., Schult, I., 1998. Optical properties of aerosols and clouds: the software package OPAC. Bull. Am. Meteorol. Soc. 79, 831–844.

Holben, B.N., Tanré, D., Smirnov, A., Eck, T.F., Slutsker, I., Abuhassan, N., Newcomb, W.W., Schafer, J.S., Chatenet, B., Lavenu, F., Kaufman, Y.J., Castle, J.V., Setzer, A., Markham, B., Clark, D., Frouin, R., Halthore, R., Karneli, A., O'Neill, N.T., Pietras, C., Pinker, R.T., Voss, K., Zibordi, G., 2001. An emerging ground-based aerosol climatology: aerosol optical depth from AERONET. J. Geophys. Res. 106, 12067–12097.

IPCC, 2021. In: Masson-Delmotte, V., Zhai, P., Pirani, A., Connors, S.L., Péan, C., Berger, S., Caud, N., Chen, Y., Goldfarb, L., Gomis, M.I., Huang, M., Leitzell, K., Lonnoy, E., Matthews, J.B.R., Maycock, T.K., Waterfield, T., Yelekçi, O., Yu, R., Zhou, B. (Eds.), Summary for Policymakers in *Climate Change 2021: the Physical Science Basis.* Contribution of Working Group I to the Fifth Assessment Report of the Intergovernmental Panel on Climate Change. Cambridge University Press, pp. 1–41.

Jethva, H., Torres, O., Ahn, C., 2014. Global assessment of OMI aerosol single-scattering albedo using ground-based AERONET inversion. J. Geophys. Res. 119, 9020–9040. https://doi.org/10.1002/2014JD021672.

Jethva, H., Chand, D., Torres, O., Gupta, P., Lyapustin, A., Patadia, F., 2018. Agricultural burning and air quality over northern India: a synergistic analysis using NASA's A-train satellite data and ground measurements, aero. Air Qual. Res. 18, 1756–1773. https://doi.org/10.4209/aaqr.2017.12.0583.

Jimenez, J.L., Canagaratna, M.R., Donahue, N.M., Prevot, A.S.H., Zhang, Q., Kroll, J.H., DeCarlo, P.F., Allan, J.D., Coe, H., Ng, N.L., Aiken, A.C., Docherty, K.S., Ulbrich, I.M., Grieshop, A.P., Robinson, A.L., Duplissy, J., Smith, J.D., Wilson, K.R., Lanz, V.A., Hueglin, C., Sun, Y.L., Tian, J., Laaksonen, A., Raatikainen, T., Rautiainen, J., Vaattovaara, P., Ehn, M., Kulmala, M., Tomlinson, J.M., Collins, D.R., Cubison, M.J., Dunlea, E.J., Huffman, J.A., Onasch, T.B., Alfarra, M.R., Williams, P.I., Bower, K., Kondo, Y., Schneider, J., Drewnick, F., Borrmann, S., Weimer, S., Demerjian, K., Salcedo, D., Cottrell, L., Griffin, R., Takami, A., Miyoshi, T., Hatakeyama, S., Shimono, A., Sun, J.Y., Zhang, Y.M., Dzepina, K., Kimmel, J.R., Sueper, D., Jayne, J.T., Herndon, S.C., Trimborn, A.M., Williams, L.R., Wood, E.C., Middlebrook, A.M., Kolb, C.E., Baltensperger, U., Worsnop, D.R., 2009. Evolution of organic aerosols in the atmosphere. Science 326, 1525–1529.

Kedia, S., Ramachandran, S., Tripathi, S.N., Holben, B., 2014. Quantification of aerosol type, and sources of aerosols over the indo-gangetic plain. Atmos. Environ. 98, 607–619. https://doi.org/10.1016/j.atmosenv.2014.09.022.

Kirillova, E.N., Marinoni, A., Bonasoni, P., Vuillermoz, E., Facchini, M.C., Fuzzi, S., Decesari, S., 2016. Light absorption properties of brown carbon in the high himalayas. J. Geophys. Res. 121. https://doi.org/10.1002/2016JD025030.

Krishnan, R., Shrestha, A.B., Ren, G., Rajbhandari, R., Saeed, S., Sanjay, J., Syed, M.A., Vellore, R., Xu, Y., You, Q., Ren, Y., Dimri, A.P., Lutz, A., Singh, P., Sun, X., Zhan, Y., 2019. In: Wester, P., Mishra, A., Mukherji, A., Shrestha, A.B. (Eds.), Unravelling Climate Change in the Hindu Kush Himalaya: Rapid Warming in the Mountains and Increasing Extremes in the Hindu Kush Himalaya Assessment, pp. 57–97.

Lawrence, M.G., Lelieveld, J., 2010. Atmospheric pollutant outflow from southern Asia: a review. Atmos. Chem. Phys. 10, 11017–11096. https://doi.org/10.5194/acp-10-11017-2010.

Levy, R.C., Mattoo, S., Munchak, L.A., Remer, L.A., Sayer, A.M., Patadia, F., Hsu, N.C., 2013. The collection 6 MODIS aerosol products over land and ocean. Atmos. Meas. Tech. 6, 2989–3034.

Li, J., Carlson, B.E., Yung, Y.L., Lv, D., Hansen, J., Penner, J.E., Liao, H., Ramaswamy, V., Kahn, R.A., Zhang, P., Dubovik, O., Ding, A., Lacis, A.A., Zhang, L., Dong, Y., 2022. Scattering and absorbing aerosols in the climate system. Nat. Rev. Earth Environ. 3, 363–379. https://doi.org/10.1038/s43017-022-00296-7.

Lüthi, Z.L., Skerlak, B., Kim, S.W., Lauer, A., Mues, A., Rupakheti, M., Kang, S.C., 2015. Atmospheric brown clouds reach the Tibetan Plateau by crossing the himalayas. Atmos. Chem. Phys. 15, 6007–6021. https://doi.org/10.5194/acp-15-6007-2015.

Mahata, K.S., Rupakheti, M., Panday, A.K., Bhardwaj, P., Naja, M., Singh, A., Mues, A., Cristofanelli, P., Pudasainee, D., Bonasoni, P., Lawrence, M.G., 2018. Observation and analysis of spatiotemporal characteristics of surface ozone and carbon monoxide in the kathmandu valley, Nepal. Atmos. Chem. Phys. 18, 14113–14132. https://doi.org/10.5194/acp-18-14113-2018.

Mallet, M., Dubovik, O., Nabat, P., Dulac, F., Kahn, R., Sciare, J., Paronis, D., Léon, J.F., 2013. Absorption properties of mediterranean aerosols obtained from multi-year ground-based remote sensing observations. Atmos. Chem. Phys. 13, 9195–9210. https://doi.org/10.5194/acp-13-9195-2013.

Maurer, J.M., Schaefer, J.M., Rupper, S., Corely, A., 2019. Acceleration of ice loss across the himalayas over the past 40 years. Sci. Adv. 5. https://doi.org/10.1126/sciadv.aav7266 eaav7266.

Myhre, G., Samset, B.H., Schulz, M., Balkanski, Y., Bauer, S., Berntsen, T.K., Bian, H., Bellouin, N., Chin, M., Diehl, T., Easter, R.C., Feichter, J., Ghan, S.J., Hauglustaine, D., Iversen, T., Kinne, S., Kirkevåg, A., Lamarque, J.-F., Lin, G., Liu, X., Lund, M.T., Luo, G., Ma, X., van Noije, T., Penner, J.E., Rasch, P.J., Ruiz, A., Seland, Ø., Skeie, R.B., Stier, P., Takemura, T., Tsigaridis, K., Wang, P., Wang, Z., Xu, L., Yu, H., Yu, F., Yoon, J.-H., Zhang, K., Zhang, H., Zhou, C., 2013. Radiative forcing of the direct aerosol effect from AeroCom phase II simulations. Atmos. Chem. Phys. 13, 1853–1877. https://doi.org/10.5194/acp-13-1853-2013.

O'Neill, N.T., Eck, T.F., Smirnov, A., Holben, B.N., Thulasiraman, S., 2003. Spectral discrimination of coarse and fine mode optical depth. J. Geophys. Res. 108. https://doi.org/10.1029/2002JD002975.

Pani, S.K., Lin, N.-H., Chantara, S., Wang, S.-H., Khamkaew, C., Prapamontol, T., Janjai, S., 2018. Radiative response of biomass-burning aerosols over an urban atmosphere in northern peninsular southeast Asia. Sci. Total Environ. 633, 892–911. https://doi.org/10.1016/j.scitotenv.2018.03.204.

Putero, D., Marinoni, A., Bonasoni, P., Calzolari, F., Rupakheti, M., Cristofanelli, P., 2018. Black carbon and ozone variability at the Kathmandu Valley and at the southern Himalayas: a comparison between a “hot spot” and a downwind high-altitude site. Aero. Air Qual. Res. 18, 623–635. https://doi.org/10.4209/aaqr.2017.04.0138.

Raatikainen, T., Hyvärinen, A.-P., Hatakka, J., Panwar, T.S., Hooda, R.K., Sharma, V.P., Lihavainen, H., 2014. The effect of boundary layer dynamics on aerosol properties at the indo-gangetic plains and at the foothills of the himalayas. Atmos. Environ. 89, 548–555. https://doi.org/10.1016/j.atmosenv.2014.02.058.

Ramachandran, S., Kedia, S., 2012. Radiative effects of aerosols over indo-gangetic plains: environmental (urban vs. rural) and seasonal variations. Environ. Sci. Pollut. Res. 19, 2159–2171. https://doi.org/10.1007/s11356-011-715-x.

Ramachandran, S., Rupakheti, M., Lawrence, M.G., 2020. Black carbon dominates the aerosol absorption over the indo-gangetic plains and the himalayan foothills, env. Int 142, 105814. https://doi.org/10.1016/j.envint.2020.105814.

Ramanathan, V., Ramana, M.V., Roberts, G., Kim, D., Corrigan, C., Chung, C., Winker, D., 2007. Warming trends in Asia amplified by brown cloud absorption. Nature 448, 575–579.

Rupakheti, D., Kang, S., Rupakheti, M., Cong, Z., Panday, A.K., Holben, B.N., 2019. Identification of absorbing aerosol types at a site in the northern edge of indo-Gangetic Plain and a polluted valley in the foothills of the central himalayas. Atmos. Res. 223, 15–23. https://doi.org/10.1016/j.atmosres.2019.03.003.

Rupakheti, D., Rupakheti, M., Abdullaev, S.F., Yin, X., Kang, S., 2020. Columnar aerosol properties and radiative effects over Dushanbe, Tajikistan in central Asia. Environ. Pol. 265, 114872. https://doi.org/10.1016/j.envpol.2020.114872.

Russell, P.B., Bergstrom, R.W., Shinozuka, Y., Clarke, A.D., DeCarlo, P.F., Jimenez, J.L., Livingston, J.M., Redemann, J., Dubovik, O., Strawa, A., 2010. Absorption angstrom exponent in AERONET and related data as an indicator of aerosol composition. Atmos. Chem. Phys. 10, 1155–1169. https://doi.org/10.5194/acp-10-1155-2010.

Russell, P.B., Kacenelenbogen, M., Livingston, J.M., Hasekamp, O.P., Burton, S.P., Schuster, G.L., Johnson, S.J., Knobelspiesse, K.D., Redemann, J., Ramachandran, S., Holben, B.N., 2014. A multiparameter aerosol classification method and its application to retrievals from spaceborne polarimetry. J. Geophys. Res. 119, 9838–9863. https://doi.org/10.1002/2013JD021411.

Saikawa, E., Panday, A., Kang, S., Gautam, R., Zusman, E., Cong, Z., Somanathan, E., Adikary, B., Yokelson, R.E., Crawford, J.H., Rupakheti, M., Ye, W.L., Saroar, M.G., 2019. In: Wester, P., Mishra, A., Mukherji, A., Shrestha, A.B. (Eds.), Air Pollution in the Hindu Kush Himalaya in the Hindu Kush Himalaya Assessment. Springer, pp. 339–377.

Schutgens, N., Tsyro, S., Gryspeerdt, E., Goto, D., Weigum, N., Schulz, M., Stier, P., 2017. On the spatio-temporal representativeness of observations. Atmos. Chem. Phys. 17, 9761–9780. https://doi.org/10.5194/acp-17-9761-2017.

Shindell, D.T., Lamarque, J.-F., Schulz, M., Flanner, M., Jiao, C., Chin, M., Young, P.J., Lee, Y.H., Rotstayn, L., Mahowald, N., Milly, G., Faluvegi, G., Balkanski, Y., Collins, W.J., Conley, A.J., Dalsoren, S., Easter, R., Ghan, S., Horowitz, L., Liu, X., Myhre, G., Nagashima, T., Naik, V., Rumbold, S.T., Skeie, R., Sudo, K., Szopa, S., Takemura, T., Voulgarakis, A., Yoon, J.-H., Lo, F., 2013. Radiative forcing in the ACCMIP historical and future climate simulations. Atmos. Chem. Phys. 13, 2939–2974. https://doi.org/10.5194/acp-13-2939-2013.

Singh, A., Mahata, K.S., Rupakheti, M., Junkermann, W., Panday, A.K., Lawrence, M.G., 2019. An overview of airborne measurement in Nepal – part 1: vertical profile of aerosol size, number, spectral absorption, and meteorology. Atmos. Chem. Phys. 19, 245–258. https://doi.org/10.5194/acp-19-245-2019.

Thompson, L.G., Thompson, E.-M., Davis, M.E., Lin, P.-N., Henderson, K., Mashiotta, T. A., 2003. Tropical glacier and ice core evidence of climate changes on annual to millennial time scales. Clim. Change 59, 137–155.

Tripathee, L., Kang, S., Rupakheti, D., Cong, Z., Zhang, Q., Huang, J., 2017. Chemical characteristics of soluble aerosols over the central himalayas: insight into spatiotemporal variations and sources. Environ. Sci. Pollut. Res. 24, 24454–24472. https://doi.org/10.1007/s11356-017-0077-0.

Zhang, Q., Zheng, Y., Tong, D., Shao, M., Wang, S., Zhang, Y., Xu, X., Wang, J., He, H., Liu, W., Ding, Y., Lei, Y., Li, J., Wang, Z., Zhang, X., Wang, Y., Cheng, J., Liu, Y., Shi, Q., Yan, L., Geng, G., Hong, C., Li, M., Liu, F., Zheng, B., Cao, J., Ding, A., Gao, J., Fu, Q., Huo, J., Liu, B., Liu, Z., Yang, F., He, K., Hao, J., 2019. Drivers of improved $PM_{2.5}$ air quality in China from 2013 to 2017. Proc. Natl. Acad. Sci. 116, 24463–24469. https://doi.org/10.1073/pnas.1907956116.